

The discovery channel at the Neutrino Factory: $\nu_\mu \rightarrow \nu_\tau$ pointing to sterile neutrinos

Andrea Donini,^a Ken-ichi Fuki,^c J. López-Pavón,^a
Davide Meloni^b and Osamu Yasuda^c

^a*Instituto Física Teórica UAM/CSIC, Cantoblanco, E-28049 Madrid, Spain*

^b*I.N.F.N., Sezione di Roma III and Università degli Studi di "Roma Tre",
Dipartimento di Fisica Via Vasca Navale 84, I-00146 Rome, Italy*

^c*Tokyo Metropolitan University, Department of Physics, Minami-Osawa 1-1
Hachioji, Tokyo 192-0397, Japan*

Abstract

We study the potential of a Neutrino Factory in constraining the parameter space of a scheme with one sterile neutrino separated from three active ones by an $\mathcal{O}(1)$ eV^2 mass-squared difference. We present approximated analytic expressions for the oscillation probabilities, showing that the greatest sensitivity to sterile neutrinos at a Neutrino Factory can be achieved using the $\nu_\mu \rightarrow \nu_\mu$ and the $\nu_\mu \rightarrow \nu_\tau$ oscillations. The latter channel, that will be called "the discovery channel", is found to be the single most sensitive channel to look for deviation from the standard three-flavor oscillation. We have performed a thorough numerical analysis of the sensitivity to sterile neutrinos of a 50 GeV Neutrino Factory with two detectors of the Hybrid-MIND type (a magnetized ECC next to a Magnetized Iron Calorimeter) located at $L = 3000$ km and $L = 7500$ km from the source. Four channels have been used: $\nu_e \rightarrow \nu_\mu, \nu_\tau$; $\nu_\mu \rightarrow \nu_\mu, \nu_\tau$. The relevant backgrounds, efficiencies and systematic errors have been taken into account. We have found that this setup can constrain $\sin^2 2\theta_{13}^{4fam} \leq 2.5 \times 10^{-5}$; $\theta_{34} \leq 10^\circ$; and $\theta_{24} \leq 6^\circ$. Our results hold for any value of $\Delta m_{\text{SBL}}^2 \gtrsim 0.1 \text{ eV}^2$. We have compared our results with those that can be obtained using a 20 GeV ISS-inspired Neutrino Factory setup, with the same detectors at $L = 4000$ km and $L = 7500$ km, finding worse sensitivities to active-sterile mixing angles ($\theta_{24} \leq 7.5^\circ$ and $\theta_{34} \leq 13^\circ$). Eventually we have shown that, if a positive signal is found, the proposed setup is able to measure simultaneously θ_{34} and δ_3 with a precision of few degrees and few tens of degrees, respectively, solving the so-called "intrinsic" and "sign degeneracies".

1 Introduction

From the results of solar [1–8], atmospheric [9,10], reactor [11–14] and accelerator [15–18] neutrino experiments, we now know that neutrinos have masses and mixings. In the framework of three flavor oscillations, neutrino oscillations are described by three mixing angles, θ_{12} , θ_{13} , θ_{23} , and one CP phase δ , as well as two independent mass-squared differences, Δm_{21}^2 and Δm_{31}^2 . In the standard parametrization [19] for the three flavor mixing matrix U_{PMNS} [20–23], when θ_{13} is small, $(\Delta m_{21}^2, \theta_{12})$ and $(\Delta m_{31}^2, \theta_{23})$ correspond to the mass-squared difference and the mixing angle of the solar and atmospheric oscillations, respectively. From the solar neutrino experiments we have $\Delta m_{\text{sol}}^2 \simeq 7.7 \times 10^{-5} \text{ eV}^2$, $\sin^2 \theta_{12} \simeq 0.30 - 0.31$ [24,25], and from the atmospheric neutrino experiments $|\Delta m_{\text{atm}}^2| \simeq 2.4 \times 10^{-3} \text{ eV}^2$, $\sin^2 2\theta_{23} \simeq 0.47 - 0.50$ [24,25]. As for θ_{13} , the reactor data [11–13] and three-family global analysis of the experimental data give an upper bound¹, $\sin^2 \theta_{13} \leq 0.04$, while we have no information on δ at present

¹ In Refs. [26,25,27], a global analysis of the neutrino oscillation data has been shown, in which a non-vanishing value for θ_{13} is found. This result, however, is compatible with $\theta_{13} = 0$ at less than 2σ , and it has not been confirmed by the other groups performing global fits [24].

(see, however, Ref. [28]).

In order to determine precisely the remaining two parameters θ_{13} and δ , long baseline experiments with intense neutrino beams have been proposed [29–35]. As in the case of the B factories [36,37], these precision measurements will allow us to look for deviation from the standard three flavor oscillations scenario. Possible scenarios for such deviations include non-standard interactions which affects the neutrino productions and detections [38], those which modify the neutrino propagations [39,40], light sterile neutrinos [22], unitarity violation due to the effect of heavy fermions [41,42], etc. These scenarios (except non-standard interactions which change the neutrino propagation, only), in general break unitarity. As in the B physics, test of unitarity is one of the important problems which should be investigated in the future long baseline experiments (see Ref. [43] for a review). Among the proposed long baseline experiments with high intense neutrino beams, a Neutrino Factory [34], which uses a muon storage ring to produce neutrino beams from muon decays, is expected to have excellent sensitivity to θ_{13} and δ . One of the advantages of a Neutrino Factory is that the flux is flavor-rich, well under control and with no ν_τ contamination. This last point is of particular relevance for new physics searches in neutrino oscillations, since oscillations into ν_τ 's provide the best signal of non-standard physics in oscillations (as it will be shown in Sect. 2.4 for sterile neutrinos; see also Refs. [44–46]) and ν_τ detection is important to check unitarity of the PMNS matrix (although, clearly, unitarity violations of the PMNS matrix are best studied in weak decay processes, [41]).

A Neutrino Factory with high energy muons is, thus, a powerful facility to look for τ 's signals, if detectors dedicated to τ -detection are provided. Notice that oscillations into ν_τ cannot be measured by so-called β beams [35] and that high energy conventional superbeams are affected by ν_τ contamination of the flux (through B -mesons decay).

Four neutrino mass schemes have attracted much attention since the announcement by the LSND group on evidence for neutrino oscillations $\bar{\nu}_\mu \rightarrow \bar{\nu}_e$ with a mass squared difference $\Delta m^2 \sim O(1) \text{ eV}^2$ [47–49]. Because the mass squared difference suggested by the LSND result is much larger than those for the solar and atmospheric neutrino oscillations, in order to explain all these data in terms of neutrino oscillations, it is necessary to introduce *at least* a fourth light neutrino state. From the LEP data [19,50], which indicate that the number of weakly interacting light neutrinos is three, the fourth state has to be a sterile neutrino. For this reason, the LSND signal could be considered as an evidence for the existence of a sterile neutrino. Recently the MiniBooNE experiment [51] gave a negative result for neutrino oscillations with the mass squared difference $\Delta m^2 \sim O(1) \text{ eV}^2$ which was suggested by the LSND data, and it has become difficult for four neutrino models to explain the LSND data. The so-called (3+2)-scheme with two sterile neutrinos has also been proposed [52] to account for LSND, but also in this case, tension with the disappearance experiments remains, as long as we take into account the LSND data. Adding a third sterile neutrino does not seem to help [53], and in general global analyses seem to indicate that sterile neutrinos alone are not enough to account for all the data in terms of neutrino oscillations. Models with sterile

neutrinos and exotic physics have been therefore proposed [54–58].

While the efforts to account for all the data including the LSND in terms of neutrino oscillations have been unsuccessful, sterile neutrino scenarios which satisfy all the experimental constraints *except* LSND are still possible. Even if the inclusion of light sterile neutrinos is not needed to explain the present experimental data, it is certainly worth investigating scenarios where sterile neutrinos do appear and constrain their parameter space. Light singlet fermions are indeed present in the low-energy spectrum of many theories and models including them represent, for example, phenomenologically natural frameworks to break three flavor unitarity.

In Ref. [59] the (3+1)-scheme without imposing the LSND constraint was studied in the context of the CNGS experiments [60], finding that if the OPERA detector is exposed to the nominal CNGS beam intensity, a null result can improve a bit the present bound on θ_{13} , but not those on the active-sterile mixing angles, θ_{14} , θ_{24} and θ_{34} .

In this paper, we have extended the analysis in Ref. [59] to the case of a Neutrino Factory experiment. We have first of all extended the analytic computation of the oscillation probabilities for the (3 + 1)-model at long baseline experiments in matter using the formalism by Kimura-Takamura-Yokomakura (KTY) [61,62]. Approximated formulæ in powers of θ_{13} , of the deviations from maximality of θ_{23} ($\delta\theta_{23}$) and of the active-sterile mixing angles, θ_{i4} , have been obtained. On the basis of this analysis, we have found that the greatest sensitivity to the active-sterile mixing angles is achieved using the $\nu_\mu \rightarrow \nu_\mu$ and $\nu_\mu \rightarrow \nu_\tau$ channels (as it was noticed, for example, in Refs. [63,64] and refs. therein). To take full advantage of these signals, detectors capable of both ν_μ and ν_τ identification are needed. In our numerical analysis we have, thus, assumed a detector of the Hybrid-MIND type [65]: a 50 kton magnetized iron calorimeter next to a 4 kton Emulsion Cloud Chamber with magnetized iron plates. This detector has a greater efficiency to $\nu_\mu \rightarrow \nu_\tau$ than the standard OPERA-type ECC, with lead plates acting as target.

We have then extensively analyzed the physics reach of a 50 GeV Neutrino Factory which has 2×10^{20} useful muon decays per year aimed at two detectors of the Hybrid-MIND type located at $L = 3000$ km and $L = 7500$ km from the source, with both polarities running for 4 years each. As a consistency check, we have also studied the case of a 20 GeV Neutrino Factory which has 5×10^{20} useful muon decays per year aimed at the same two detectors of the Hybrid-MIND type located at $L = 4000$ km and $L = 7500$ km, again with both polarities running for 4 years each. The latter option was the scenario which was suggested in the *International Scoping Study for a future Neutrino Factory and Super-Beam facility* [43].

Four signals have been considered: the "standard" Neutrino Factory channels, the golden channel $\nu_e \rightarrow \nu_\mu$ [66] and the silver channel $\nu_e \rightarrow \nu_\tau$ [67]; the ν_μ disappearance channel; and the novel signal $\nu_\mu \rightarrow \nu_\tau$, that will be named as "the discovery channel" due to its high-sensitivity to new physics signals in neutrino oscillations. Using the first two channels at the 50 GeV Neutrino Factory, we can extend the three-family θ_{13} -

sensitivity plots to the four-family $(\theta_{13}, \theta_{14})$ -plane, putting a stringent upper bound on the four-family θ_{13} mixing angle, $\sin^2 2\theta_{13} \lesssim \mathcal{O}(10^{-5})$. Using the combination of the ν_μ disappearance channel and of the "discovery channel" $\nu_\mu \rightarrow \nu_\tau$ at the 50 GeV Neutrino Factory, we are able to constrain the active-sterile mixing angles θ_{34} and θ_{24} , $|\theta_{34}| \lesssim 10^\circ$ and $|\theta_{24}| \lesssim 6^\circ$. We have found that the combination of the shortest baseline data with the longest baseline ones significantly improves the sensitivity in both planes, $(\theta_{13}, \theta_{14})$ and $(\theta_{24}, \theta_{34})$.

We have, then, compared our results for the 50 GeV Neutrino Factory with those that can be obtained at the 20 GeV ISS-inspired one, finding that the former setup has a far greater potential than the latter for sterile neutrino searches, due to the larger τ statistics that can be collected using higher energy muons.

Eventually, we have performed a very preliminary study of the potential of the 50 GeV Neutrino Factory to measure four-family parameters, showing 99% CL contours in the (θ_{34}, δ_3) -plane for fixed values of θ_{24} . We have found that the shortest baseline data give a very good precision in δ_3 , but are affected by "intrinsic" [68] and "sign" degeneracies [69]. On the other hand, the longest baseline data have a rather good precision in θ_{34} and are not affected by those degeneracies. The combination of the two baselines, thus, is able to measure simultaneously θ_{34} and δ_3 with a precision of a few degrees and a few tens of degrees, respectively.

An analysis such as this is not completely new: first studies of sterile neutrinos at a Neutrino Factory were presented at the first NuFact workshop in Lyon in 1999 [70,71] in the framework of the so-called (2+2)-schemes and subsequently extended to the case of (3+1)-schemes in Ref. [63]. The possibility to use the Neutrino Factory detectors, optimized to look for three-family oscillations, to disentangle three- from four-neutrino signals was considered in Ref. [72,64]. Recently, in Ref. [73] a four-family neutrino analysis in the spirit of Ref. [59] has been performed. The main differences between this paper and Ref. [73] are (i) that careful numerical analyses are carried out here by taking into account backgrounds, efficiencies and systematic errors specific to the considered signals and setup, and (ii) that the four channels $\nu_\mu \rightarrow \nu_\tau$, $\nu_\mu \rightarrow \nu_\mu$, $\nu_e \rightarrow \nu_\mu$, $\nu_e \rightarrow \nu_\tau$ at the Neutrino Factory are considered and their contributions are clarified in the present paper.

The paper is organized as follows. In Sec. 2 the main features of four-neutrino schemes and the present bounds on the mixing angles in these scenarios are briefly summarized. Furthermore we compute approximated oscillation probabilities in matter in the atmospheric regime using the KTY formalism [61,62] (details of our computations are given in App. A). In Sec. 3 we remind the details of the considered Neutrino Factory setup. In Sec. 4 we present our results using various channels at the Neutrino Factory. Finally, in Sec. 5 we draw our conclusions.

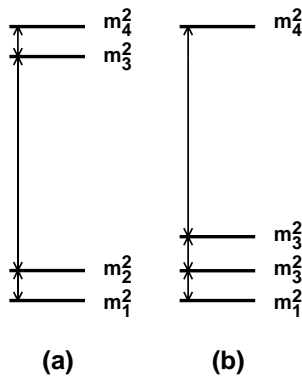


Fig. 1. The two classes of four-neutrino mass spectra, (a): (2+2) and (b): (3+1).

2 Four neutrino schemes

Four-neutrino schemes consist of one extra sterile state in addition to the three weakly interacting ones. Depending on whether one or two mass eigenstate(s) are separated from the others by the largest mass-squared gap², the schemes are called (3+1)- and (2+2)-schemes, as is shown in Fig. 1. In the (3+1) schemes, there is a group of three close-by neutrino masses that is separated from the fourth one by the larger gap. In (2+2) schemes, there are two pairs of close masses separated by the large gap. These two classes lead to very different phenomenological consequences.

2.1 (2+2)-schemes

A characteristic feature of (2+2) schemes is that the extra sterile state cannot simultaneously decouple from *both* solar and atmospheric oscillations. The fraction of sterile neutrino contributions to solar and atmospheric oscillations is given by $|U_{s1}|^2 + |U_{s2}|^2$ and $|U_{s3}|^2 + |U_{s4}|^2$, respectively, where the mass squared differences Δm_{21}^2 and $|\Delta m_{43}^2|$ are assumed to be those of the solar and atmospheric oscillations. The experimental results show that mixing among active neutrinos give dominant contributions to both the solar and atmospheric oscillations (see, e.g., Ref. [75]). In particular, in Fig. 19 of Ref. [75] we can see that at the 99% level $\eta_s \equiv |U_{s1}|^2 + |U_{s2}|^2 \leq 0.25$ and $1 - \eta_s = |U_{s3}|^2 + |U_{s4}|^2 \leq 0.25$, which contradicts the unitarity condition $\sum_{j=1}^4 |U_{sj}|^2 = 1$. In fact the (2+2)-schemes are excluded at 5.1σ CL [75]. This conclusion is independent of whether we take the LSND data into consideration or not and we will not consider (2+2)-schemes in the rest of this paper.

² The only assumption for the largest mass-squared difference is that oscillations caused by this mass-squared difference are averaged. So the results hold for any value of $\Delta m_{\text{SBL}}^2 \gtrsim 0.1 \text{ eV}^2$. Interesting models with a much heavier "sterile" neutrino, $m \sim O(1) \text{ KeV}$ can be found, for example, in Ref. [74].

2.2 (3+1)-schemes with the LSND constraint

On the other hand, (3+1)-schemes are not affected by the tension between the solar and atmospheric constraints on sterile neutrino oscillations, because as long as the mixing of sterile neutrino is small, then phenomenology of solar and atmospheric oscillations is approximately the same as that of the three flavor framework. The (3+1) schemes start having a problem only when one tries to account for LSND and all other negative results of the short baseline experiments. To explain the LSND data while satisfying the constraints from other disappearance experiments, the oscillation probabilities of the appearance and disappearance channels have to satisfy the following relation [76,77]:

$$\sin^2 2\theta_{\text{LSND}}(\Delta m^2) < \frac{1}{4} \sin^2 2\theta_{\text{Bugey}}(\Delta m^2) \cdot \sin^2 2\theta_{\text{CDHSW}}(\Delta m^2) \quad (1)$$

where $\theta_{\text{LSND}}(\Delta m^2)$, $\theta_{\text{CDHSW}}(\Delta m^2)$, $\theta_{\text{Bugey}}(\Delta m^2)$ are the value of the effective two-flavor mixing angle as a function of the mass squared difference Δm^2 in the allowed region for LSND ($\bar{\nu}_\mu \rightarrow \bar{\nu}_e$), the CDHSW experiment [78] ($\nu_\mu \rightarrow \nu_\mu$), and the Bugey experiment [79] ($\bar{\nu}_e \rightarrow \bar{\nu}_e$), respectively. The reason that the (3+1)-scheme to explain LSND is disfavored is basically because Eq. (1) is not satisfied for any value of Δm^2 . A (3+2)-scheme with two sterile neutrino has also been proposed [52] to account for LSND, and it may be possible to reconcile the LSND and MiniBooNE data by introducing a CP phase [80,53]. Also in this case, however, tension with CDHSW [78] and Bugey [79] remains, as in the case of the (3+1)-scheme.

2.3 (3+1)-schemes without the LSND constraint

If we give up our effort to account for the LSND data, on the other hand, we no longer have the constraint (1). In this case we have only the upper bound on the extra mixing angles and this scenario satisfies all the experimental constraints (except that of LSND). Throughout this work, therefore, we will consider a (3+1)-scheme without taking the LSND data into account while satisfying all the negative constraints, as it was done in Ref. [59].

It has been discussed that the mixing angles of four neutrino schemes may be constrained by big-bang nucleosynthesis (see Refs. [76,81] and references therein), and if such arguments are applied, then the mixing angles of sterile neutrinos would have to be very small. However, it is known that in some model [82] neutrino oscillations themselves create large lepton asymmetries which prevent sterile neutrinos from being in thermal equilibrium, so it is not so clear whether the arguments in [76,81] hold. At present, therefore, it is far to say that there is not yet general consensus on this issue (see Ref. [83] and references therein). In this paper we will not impose cosmological constraints on our scheme.

The mixing matrix U can be conveniently parametrized in terms of six independent

rotation angles θ_{ij} and three (if neutrinos are Dirac fermions) or six (if neutrinos are Majorana fermions) phases δ_i . In oscillation experiments, only the so-called ‘‘Dirac phases’’ can be measured, since the ‘‘Majorana phases’’ appear only as an overall phase of the oscillation amplitude and disappear in the oscillation probability. The Majorana or Dirac nature of neutrinos can thus be tested only in $\Delta L = 2$ transitions such as neutrino-less double β -decay or lepton number violating decays [19]. In the following analysis, with no loss in generality, we will restrict ourselves to the case of 4 Dirac-type neutrinos only.

A generic rotation in a four-dimensional space can be obtained by performing six different rotations along the Euler axes. Since the ordering of the rotation matrices R_{ij} (where ij refers to the plane in which the rotation takes place) is arbitrary, plenty of different parametrizations of the mixing matrix U are allowed. In this paper we are interested in the so-called ‘‘atmospheric regime’’, with oscillations driven by the atmospheric mass difference, $\Delta m_{\text{atm}}^2 L/E \sim \mathcal{O}(1)$. We will then make use of the following parametrization, adopted in Ref. [53]:

$$U = R_{34}(\theta_{34}, 0) R_{24}(\theta_{24}, 0) R_{23}(\theta_{23}, \delta_3) R_{14}(\theta_{14}, 0) R_{13}(\theta_{13}, \delta_2) R_{12}(\theta_{12}, \delta_1). \quad (2)$$

In Eq. (2), $R_{ij}(\theta_{ij}, \delta_l)$ are the complex rotation matrices in the ij -plane defined as:

$$[R_{ij}(\theta_{ij}, \delta_l)]_{pq} = \begin{cases} \cos \theta_{ij} & p = q = i, j \\ 1 & p = q \neq i, j \\ \sin \theta_{ij} e^{-i\delta_l} & p = i; q = j \\ -\sin \theta_{ij} e^{i\delta_l} & p = j; q = i \\ 0 & \text{otherwise.} \end{cases} \quad (3)$$

It is convenient to put phases in R_{12} (so that it automatically drops in the limit $\Delta_{\text{sol}} = \Delta m_{\text{sol}}^2 L/2E \rightarrow 0$) and R_{13} (so that it reduces to the ‘‘standard’’ three-family Dirac phase when sterile neutrinos are decoupled). The third phase can be put anywhere; we will place it in R_{23} . Note that in the one-mass dominance regime [84] (i.e. for $\Delta_{\text{atm}} = \Delta m_{\text{atm}}^2 L/2E, \Delta_{\text{sol}} \rightarrow 0$) all the phases automatically disappear from the oscillation probabilities for some choices of the four-family PMNS matrix parametrization.

This parametrization has been used in Ref. [59] to put bounds on the active-sterile mixing angles θ_{i4} using existing data (including MiniBooNE but neglecting LSND). These bounds can be summarized as follows:

(1) Bounds from ν_e disappearance reactor experiments

Reactor experiments such as Bugey and Chooz can put stringent bounds on θ_{13} and θ_{14} in this parametrization: $\theta_{13} \leq 13^\circ$ and $\theta_{14} \leq 10^\circ$ at 99% CL, for any value of $\Delta m_{\text{SBL}}^2 > 0.1 \text{ eV}^2$, with some correlation between the two (in particular the four-family Chooz bound on θ_{13} is slightly modulated by θ_{14}).

(2) Bounds from ν_μ disappearance experiments

A “negative” result in a ν_μ disappearance experiment at ”atmospheric” L/E (such as K2K or MINOS), in which ν_μ oscillations can be very well fitted in terms of three-family oscillations, puts a stringent bound on the mixing angle θ_{24} . The bound from such experiments found in Ref. [59] is: $\theta_{24} \leq 14^\circ$ at 99% CL, for $\Delta m_{\text{SBL}}^2 \geq 0.1 \text{ eV}^2$.

(3) Bounds on θ_{34}

Neither ν_e nor ν_μ disappearance probabilities in vacuum depend strongly on θ_{34} (as it can be seen in Ref. [59]). An upper bound on θ_{34} , however, can be drawn as the result of indirect searches for $\nu_\mu \rightarrow \nu_s$ conversion in atmospheric neutrino experiments, that take advantage of the different interaction with matter of active and sterile neutrinos. Present bounds on θ_{34} arise, thus, from a measurement of spectral distortion. On the other hand, bounds on θ_{13}, θ_{14} and θ_{24} are mainly drawn by a flux normalization measurement. As a consequence, the bound on θ_{34} that we can draw by non-observation of $\nu_\mu \rightarrow \nu_s$ oscillation in atmospheric experiments is less stringent than those we have shown before. For this reason, θ_{34} can be somewhat larger than θ_{13}, θ_{14} and θ_{24} : $\theta_{34} \leq 32^\circ$ at 99% CL.

These bounds are depicted in Fig. 2 of Ref. [59], where 90%, 95%, 99% and 3σ CL contours in the $(\theta_{13} - \theta_{14})$ - and $(\theta_{24} - \theta_{34})$ -planes are shown for $\Delta_{\text{sol}} \rightarrow 0$ and $\Delta m_{\text{atm}}^2 = 2.4 \times 10^{-3} \text{ eV}^2$ and $\theta_{23} = 45^\circ$.

In the same paper, the potential of the CNGS beam to improve those bounds was studied, finding that if the OPERA detector is exposed to the nominal CNGS beam intensity, a null result can improve a bit the present bound on θ_{13} , but not those on the active-sterile mixing angles, θ_{14}, θ_{24} and θ_{34} . If the beam intensity is increased by a factor 2 or beyond, not only the sensitivity to θ_{13} increases accordingly, but a significant sensitivity to θ_{24} and θ_{34} is achievable. The $(\theta_{24}, \theta_{34})$ combined sensitivity strongly depends on the value of the CP-violating phase δ_3 , however, with stronger sensitivity for values of δ_3 approaching 90° . Only a marginal improvement is achievable on the bound on θ_{14} , that should be constrained by high-intensity ν_e disappearance experiments.

These results are depicted in Fig. 4 of Ref. [59], where 90% and 99% CL contours in the $(\theta_{13} - \theta_{14})$ - and $(\theta_{24} - \theta_{34})$ -planes are shown for $\Delta m_{\text{sol}}^2 = 7.9 \times 10^{-5} \text{ eV}^2, \Delta m_{\text{atm}}^2 = 2.4 \times 10^{-3} \text{ eV}^2, \theta_{12} = 34^\circ, \theta_{23} = 45^\circ$ and $\delta_1 = \delta_2 = 0; \delta_3 = 0, 90^\circ$, assuming 1, 2, 3, 5 and 10 times the nominal CNGS beam intensity of 4.5×10^{19} pot/years.

2.4 Oscillation probabilities at the Neutrino Factory in the (3+1)-scheme

To understand the details of the different channels with the greatest sensitivity to the four-family neutrino schemes, it is useful to obtain simple analytical expressions for the different channels in matter. Hereafter, we will assume a constant Earth density along the neutrino path, computed using the PREM [85]. Notice that, in the framework of

Neutrino Factory experiments simulations, the impact of non-constant matter density has been thoroughly studied, showing that for the baselines and the muon energy considered in this paper the details of the density profile crossed by neutrinos does not modify the results³.

To derive the oscillation probabilities, we adopt the KTY formalism [61,62] (the details are given in the Appendix A). Furthermore, to get simplified forms of the formulæ, it is convenient to obtain the probabilities expanding with respect to the following small parameters:

$$\epsilon \equiv s_{34} \sim \sqrt{s_{13}} \sim \sqrt{s_{14}} \sim \sqrt{s_{24}} \sim \sqrt{\delta\theta_{23}} \lesssim 4 \times 10^{-1}.$$

The relevant oscillation probabilities in matter, expanded to third order in ϵ , are given by the following:

$$P_{ee} \sim 1 + \mathcal{O}(\epsilon^4), \quad (4)$$

$$P_{e\mu} \sim P_{e\tau} \sim P_{es} \sim \mathcal{O}(\epsilon^4), \quad (5)$$

$$P_{\mu\mu} = 1 - \sin^2 \frac{\Delta_{31}L}{2} - 2(A_n L) s_{24} s_{34} \cos \delta_3 \sin \Delta_{31}L + \mathcal{O}(\epsilon^4), \quad (6)$$

$$P_{\mu\tau} = \left(1 - s_{34}^2\right) \sin^2 \frac{\Delta_{31}L}{2} + \{s_{24} s_{34} \sin \delta_3 + 2(A_n L) s_{24} s_{34} \cos \delta_3\} \sin \Delta_{31}L + \mathcal{O}(\epsilon^4), \quad (7)$$

$$P_{\mu s} = s_{34}^2 \sin^2 \frac{\Delta_{31}L}{2} - s_{24} s_{34} \sin \delta_3 \sin \Delta_{31}L + \mathcal{O}(\epsilon^4), \quad (8)$$

where $\Delta_{31} = \Delta m_{31}^2/2E$, $s_{ij} = \sin \theta_{ij}$, and we take the convention that the central value of $|\Delta m_{31}^2|$ is Δm_{atm}^2 , which is determined by the two flavor analysis of the atmospheric neutrino data. The nucleon matter density parameter A_n is defined in the App. A, $A_n = \sqrt{2}G_F n_n/2$. From eqs. (4)-(8), it can be easily verified that unitarity is satisfied to this order in ϵ . As it can be seen, moreover, the ν_e decouples within this approximation. We can thus conclude that the "classic" Neutrino Factory channels, such as the "golden channel" $\nu_e \rightarrow \nu_\mu$ and the "silver channel" $\nu_e \rightarrow \nu_\tau$, are of limited interest to study sterile neutrinos (as it is known since long, see for example Refs. [63,64,59]).

The most relevant oscillation channels in this context are the ν_μ disappearance channel and the $\nu_\mu \rightarrow \nu_\tau$ appearance channel. First of all, we see that sensitivity to θ_{34} is provided by the first term in eq. (7), that is proportional to $(1 - s_{34}^2)$. Sensitivity to θ_{24} is best achieved using the $\nu_\mu \rightarrow \nu_\mu$ oscillations, though the relevant term appears at $\mathcal{O}(\epsilon^4)$. In eqs. (6)-(7) we can also see that combined sensitivity to θ_{24} and θ_{34} is achievable

³ This is totally different, for example, in the case of β -Beams with Li/B decaying ions. In those setups, a resonance is crossed for $O(5 \text{ GeV})$ neutrinos for $L = O(10000) \text{ km}$ baselines [86].

through the $O(\epsilon^3)$ matter-dependent $s_{24}s_{34} \cos \delta_3$ term. The bounds on these two angles are those that can be improved the most by the Neutrino Factory experiments. Since θ_{34} is considerably less constrained than the rest of the new angles (which are as constrained as θ_{13}), and of course it is impossible to use the "sterile appearance" channel $\nu_\mu \rightarrow \nu_s$, we can safely say that the $\nu_\mu \rightarrow \nu_\tau$ is the best option to look for a sterile neutrino signal. Eventually, the $\nu_\mu \rightarrow \nu_\tau$ channel can also test CP violation in four-family scenarios through the $O(\epsilon^3)$ matter-independent $s_{24}s_{34} \sin \delta_3$ term.

Notice that the $\nu_\mu \rightarrow \nu_\tau$ channel has not been studied in detail yet in the framework of neutrino factories studies (with the possible exceptions of Refs. [87,88]), but it is manifestly the single most important channel to study new physics [44–46], if the related experimental problems could be overcome. For this reason, we will name it throughout this paper as "*the discovery channel*".

3 The Neutrino Factory and the Hybrid-MIND detector

In a Neutrino Factory [34,89] muons are first produced with a multi-MW proton source, accelerated up to energies of several GeV's, and finally injected into a storage ring with long straight sections aiming to one or more detectors. The muon decays $\mu^+ \rightarrow e^+ \nu_e \bar{\nu}_\mu$ and $\mu^- \rightarrow e^- \bar{\nu}_e \nu_\mu$ provide a very well known two-flavor neutrino flux [90] with energies in the range $E_\nu \in [0, E_\mu]$. Neutrino Factory designs have been proposed in Europe [91,92], the US [93–96], and Japan [97]. The dedicated *International Scoping Study for a future Neutrino Factory and Super-Beam facility* [43] showed that, provided sufficient resources, an accelerator complex capable of providing about 10^{21} muon decays of a given polarity per year can be built.

The Neutrino Factory setup that we propose for sterile neutrinos searches and that we examine in detail in the rest of the paper is defined as follows: muons of both polarities are accelerated up to $E_\mu = 50$ GeV and injected into one storage ring with a geometry that allows to aim at two far detectors, the first located at 3000 km and the second at 7500 km from the source. An alternative option, considered in the final ISS Accelerator Report [98], is to inject the muon beam into different storage rings, each of them aimed to a single far detector. The number of useful muon decays per year aimed at each detector has been fixed to 2×10^{20} . This number is rather conservative since, in the final ISS Physics Report [43], with a similar storage ring(s) geometry, 5×10^{20} useful muon decays per year aimed at each detector are considered (i.e., 10^{21} total useful muon decays per year). Four years of data taking for each muon polarity are envisaged.

Notice that the adopted setup, similar to those proposed in the first Neutrino Factory studies (see, for example, Refs. [66,68]), slightly differs from the setup that was suggested in the final ISS Physics Report. The latter consists in stored muons with energies in the range $E_\mu \in [20, 30]$ GeV, aiming to two detectors located at $L = 4000$ km and $L = 7500$ km from the source. The longest baseline corresponds to the so-called "magic

baseline” [99], where three-family CP-violating effects vanish. We have chosen the same baseline for the far detector in our setup, although in the (3+1)-neutrino model not all of the CP-violating phases dependence decouple at this distance (as it can be seen from eqs. (6,7) and in Sect. 4). The shortest baseline was optimized in the ISS Physics Report to look for CP-violating three-family signals, finding that a detector with a baseline of $L = 4000$ km performed slightly better than at $L = 3000$ km. This optimization, however, is no longer valid when looking for the (3+1)-neutrino model signals. We decided, therefore, to adopt the $L = 3000$ km baseline used in previous studies, for which possible sites were already been explored⁴. Eventually, we use a stored muon energy that is larger than the optimal value adopted in the ISS Physics Report, again chosen to maximize the sensitivity to three-family observables such as θ_{13} , the sign of the atmospheric mass difference and the three-family CP-violating phase δ . It is indeed well known from previous studies (see, for example, Ref. [100] for an optimization of the muon energy to look for NSI signals at the Neutrino Factory) that to look for new physics the higher the muon energy the better. An evident motivation for this is that channels with oscillations into τ 's (the silver channel $\nu_e \rightarrow \nu_\tau$ and, more importantly, the ”discovery channel” $\nu_\mu \rightarrow \nu_\tau$) are the best ones to look for new physics in neutrino oscillations, and high neutrino energies are required to circumvent the extremely low $\nu_\tau N$ cross-section in the tens of GeV energy range.

To show that the 50 GeV Neutrino Factory setup proposed above is more suited to look for sterile neutrino signals, we will compare our results with an ISS-inspired Neutrino Factory, defined as follows: muons of both polarities are accelerated up to $E_\mu = 20$ GeV and injected into storage ring(s) with a geometry that allows to aim at two far detectors, the first located at 4000 km and the second at 7500 km from the source. The number of useful muon decays per year aimed at each detector has been fixed in this case to 5×10^{20} , following the final ISS Physics Report [43]. Four years of data taking for each muon polarity are envisaged.

The Neutrino Factory fluxes (for μ^- accumulated in the storage ring) at $L = 3000$ km as a function of the neutrino energy for $E_\mu = 50$ GeV are shown in Fig. 2(left).

Two detectors of different technologies have been considered to look for the ν_μ disappearance and for the $\nu_\mu \rightarrow \nu_\tau$ signals. The first one is a magnetized iron calorimeter [103], that was proposed in a slightly different form in Ref. [104] to measure the ”golden” $\nu_e \rightarrow \nu_\mu$ wrong-sign muons signal. The second detector is a Magnetized Emulsion Cloud Chamber (MECC) [65], an evolution of the ECC modeled after OPERA that was first considered for Neutrino Factory studies in Refs. [67,105] to look for the ”silver channel” $\nu_e \rightarrow \nu_\tau$ (a channel that can be looked at only in a Neutrino Factory setup). We consider the same detectors when studying the performance of the ISS-inspired 20 GeV setup.

⁴ For example, the island of La Palma in the Canary Islands, the island of Longyearbyen in Norway or the Oulu mine in Pyhösalmi in Finland are possible options for the location of a detector at approximately 3000 km from the source for a CERN-based Neutrino Factory.

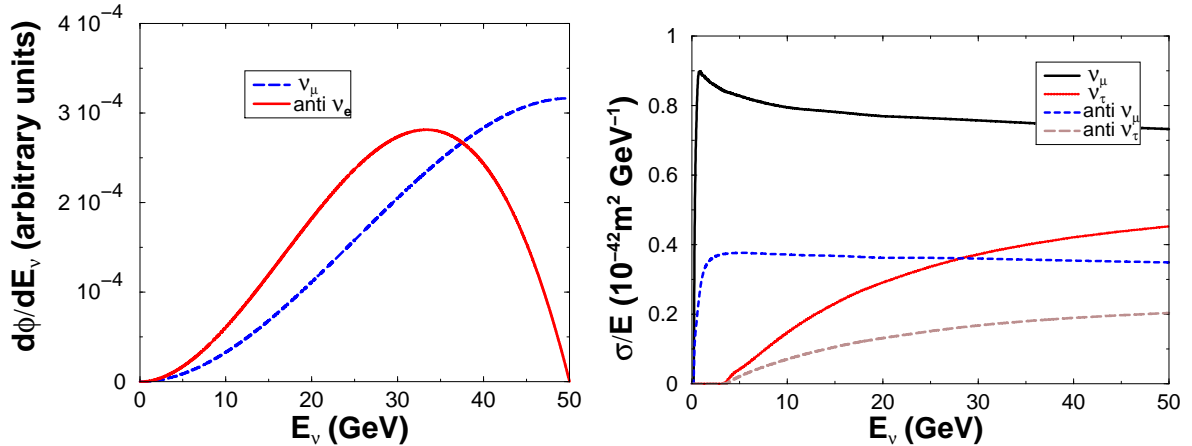


Fig. 2. *Left: 50 GeV Neutrino Factory fluxes at $L = 3000$ km; Right: the $\nu_\mu N$ and $\nu_\tau N$ cross-sections on iron [101,102].*

The $\nu_\mu N$ and $\nu_\tau N$ cross-sections on iron as a function of the neutrino energy for both neutrinos and anti-neutrinos are shown in Fig. 2(right).

3.1 The MIND detector: $\nu_e \rightarrow \nu_\mu$ and $\nu_\mu \rightarrow \nu_\mu$

The baseline detector, a 50 kton magnetized iron calorimeter of the MINOS type, was originally optimized to reduce the background to the wrong-sign muon signal for $\nu_e \rightarrow \nu_\mu$ oscillations (represented dominantly by right-sign muons with a wrong charge assignment and charmed meson decays) to the 10^{-6} level. To achieve this extremely ambitious signal-to-background ratio, tight kinematical cuts were applied. Such cuts, although strongly reducing the background, have the disadvantage of an important suppression of the signal below 10 GeV, an energy region that, on the other hand, has been shown to be extremely important. A non-negligible signal below and above the first oscillation peak (that, for $L \sim 3000$ km, lies precisely in this energy range) is crucial to solve many of the parametric degeneracies [68,69,106,107] that bother the three-family (θ_{13}, δ) -measurement. To reduce such problems, a modification of the original detector proposal called MIND (Magnetized Iron Neutrino Detector) was presented in Ref. [103].

Studies of the four-family $\nu_e \rightarrow \nu_\mu$ oscillation (still the best channel to measure θ_{13}) are not different from those performed in the framework of the three-family model. In particular, no new sources of background are expected. Quite the contrary, those backgrounds induced by wrongly reconstructed $\bar{\nu}_\mu$ are expected to decrease for large values of θ_{34} , due to the increased oscillation into sterile neutrinos, see eq. (8). When looking at $\nu_e \rightarrow \nu_\mu$ oscillations, we will therefore take advantage of the wrong-sign muon identification efficiency presented in the ISS Detector Report [65]: $\epsilon_{e\mu} = 0.7$ above 10 GeV, with the efficiency increasing linearly from $\epsilon_{e\mu} = 0.1$ at 1 GeV.

The MIND detector can also be used to look for $\nu_\mu \rightarrow \nu_\mu$ disappearance (one of the channels of interest to study sterile neutrino models), providing a very good measure-

ment of the atmospheric parameters θ_{23} and Δm_{atm}^2 and giving some handle to solve the “octant degeneracy” (see, e.g., Ref. [87,108]). For the right-sign muon sample there is no need to accurately tell the charge of the muon, since the background induced by misidentified wrong-signs muons is negligible with respect to the signal, [109]. We can safely use for this signal the muon identification efficiency of the MINOS experiment [110]: $\epsilon_{\mu\mu} = 0.9$ above 1 GeV. The background in this case is represented by 10^{-5} of all neutral current events and *all* wrong-sign muon events. We have checked that the inclusion of this background has no effect on our results.

Notice that at the MIND detector it is not possible to single out τ 's decaying to muons. We cannot thus use MIND to study the leading $\nu_\mu \rightarrow \nu_\tau$ oscillation and the “silver” $\nu_e \rightarrow \nu_\tau$ channel.

Different treatments of the energy response of the detector can be found. For example, in Ref. [66] a constant energy resolution $\Delta E_\nu = 0.2E_\mu$ was considered, by grouping events in five bins of energy width $\Delta E_\nu = 10$ GeV. On the other hand, in Ref. [111] a finer binning was adopted, with a more refined treatment of the energy resolution: 43 bins of variable ΔE_ν were considered in the energy range $E_\nu \in [1\text{GeV}, E_\mu]$, folding the event distribution with a Gaußian resolution kernel of variable width, $\sigma_E = 0.15 \times E_\nu$. In this paper we have followed the first approach, grouping events into 10 constant energy resolution bins with $\Delta E_\nu = 0.1E_\mu$, leaving possible improvements of the detector simulation following Ref. [111] (if needed) for future publications.

Global 2% and 5% systematic errors on the golden channel and on the ν_μ disappearance signal, respectively, have been considered throughout our numerical simulations.

Notice that a different proposal for a magnetized iron calorimeter that can be used for a Neutrino Factory experiment has been advanced in Ref. [112].

3.2 The MECC detector: $\nu_e \rightarrow \nu_\tau$ and $\nu_\mu \rightarrow \nu_\tau$

Two technologies were considered in the literature to study neutrino oscillations into τ 's: Liquid Argon detectors [87,88] and Emulsion Cloud Chamber techniques. In both cases, the $\nu_e, \nu_\mu \rightarrow \nu_\tau$ signal can be tagged looking for right-sign muons in coincidence with a τ decay vertex, to distinguish them from ν_μ disappearance muons. Therefore, a detector with muon charge identification and vertex reconstruction is needed.

A dedicated analysis to use an ECC modeled after OPERA at the Neutrino Factory to look for the “silver channel” $\nu_e \rightarrow \nu_\tau$ [67] has been published in Ref. [105]. In that reference, a 5 kton ECC was considered, with a detailed study of the main sources of background.

The result of that analysis was that τ 's can be identified with a very low background, at the price of a very low efficiency, $O(5\%)$. One of the main motivation of such low efficiency was that only the $\tau \rightarrow \mu$ decay channel was used, i.e. only 17% of the total amount of produced τ 's. In the OPERA detector used at the CNGS and in the analysis

of Ref. [105], the τ charge identification is achieved using two large spectrometers located at the end of two thick active sections, with bricks made of repeated layers of lead (acting as the target for $\nu_\tau N$ interactions) and emulsions. In the Magnetized ECC (MECC) proposal [65] the lead plates are replaced by iron plates, again interleaved with emulsions layers. The ECC can be, thus, directly magnetized through the iron plates. Emulsion spectrometers (currently in their test phase, [113]) are located at the end of the ECC section. Eventually, the MECC is placed in front of the MIND detector, to form the so-called Hybrid-MIND setup. The efficiency of this detector to τ 's is much higher than in the case of the standard ECC, since τ decay into electrons and into hadrons can be used in addition to $\tau \rightarrow \mu$ decays. The expected efficiency is, thus, approximately five times larger than in the case of the ECC (see, for example, Refs. [65,114] and refs. therein).

The MECC bricks are bigger than the corresponding ECC ones, due to the replacement of the lead target with iron. The huge volume to be magnetized put, thus, a tight limit on the maximum foreseeable detector mass. We will therefore consider throughout the paper a 4 kton MECC [115] located in front of the 50 kton MIND, and use this detector to study both the silver channel $\nu_e \rightarrow \nu_\tau$ and the novel "discovery channel" $\nu_\mu \rightarrow \nu_\tau$. For the silver channel signal, we will use an energy dependent efficiency $\epsilon_{e\tau}$ taken from Ref. [105], multiplying it by a factor five to take into account that all τ 's decay channel can be used at the MECC. A detailed study of the efficiency to the $\nu_\mu \rightarrow \nu_\tau$ channel at the MECC, on the other hand, is lacking. We will therefore assume a constant efficiency $\epsilon_{\mu\tau} = 0.65$ above 5 GeV, increasing by a factor five the efficiency considered in Ref. [59]. This assumption must be checked in further studies of the MECC-type detectors exposed to a Neutrino Factory beam.

The backgrounds for the silver and the discovery channels should be also correspondingly increased at the MECC with respect to the ECC ones. At the ECC, the expected signal-to-background ratio (after some kinematical cuts) for $\nu_\mu \rightarrow \nu_\tau$ (using the $\tau \rightarrow \mu$ decay channel, only) is 50:1 or larger [59], the dominant source of background for the process $\nu_\mu \rightarrow \nu_\tau \rightarrow \tau^- \rightarrow \mu^-$ being represented by non-oscillated muons that produce charmed mesons eventually decaying into μ^- either through NC or CC in which the muon is not observed. No detailed study of the expected background for the $\nu_e \rightarrow \nu_\tau$ or the $\nu_\mu \rightarrow \nu_\tau$ signals at the MECC exposed to a Neutrino Factory beam has been performed yet, though. We have thus decided to make the assumption that, using MECC, all τ decay channels should be affected by similar backgrounds. We have therefore consistently multiplied the backgrounds for $\nu_e \rightarrow \nu_\tau$ and $\nu_\mu \rightarrow \nu_\tau$ computed in Refs. [105,59] by a factor five. This is possibly a conservative assumption⁵, since the MECC is expected to have a signal-to-background ratio for this signal slightly better

⁵ Notice that, for the silver channel, at least the background induced by right-sign τ 's with wrong charge assignment should be depleted in a four-family neutrino scenario with respect to the standard three-family one. This particular background is strongly affected by active-sterile mixing angles, since, in the allowed region of the parameter space, $\nu_\mu \rightarrow \nu_\tau$ oscillations are significantly depleted with respect to the standard three-neutrino ones.

$(\theta_{13}; \theta_{14}; \theta_{24}; \theta_{34})$	$N_{\tau^-}^{CNGS}$	$N_{\tau^-}^{3000}$	$N_{\tau^+}^{3000}$	$N_{\tau^-}^{7500}$	$N_{\tau^+}^{7500}$
$(5^\circ; 5^\circ; 5^\circ; 20^\circ)$	8.9	559	10	544	2
$(5^\circ; 10^\circ; 5^\circ; 20^\circ)$		557	29	544	5
$(5^\circ; 5^\circ; 10^\circ; 20^\circ)$	8.3	474	11	529	2
$(5^\circ; 5^\circ; 10^\circ; 30^\circ)$	10.5	384	18	454	3
$(5^\circ; 10^\circ; 5^\circ; 30^\circ)$		424	59	441	11
$(5^\circ; 5^\circ; 10^\circ; 30^\circ)$	10.5	384	18	454	3
$(10^\circ; 5^\circ; 5^\circ; 20^\circ)$	8.5	522	22	512	2
$(10^\circ; 10^\circ; 5^\circ; 20^\circ)$		517	42	510	6
$(10^\circ; 5^\circ; 10^\circ; 20^\circ)$	7.9	443	22	498	2
$(10^\circ; 5^\circ; 5^\circ; 30^\circ)$	6.5	397	30	413	4
$(10^\circ; 10^\circ; 5^\circ; 30^\circ)$		389	74	412	11
$(10^\circ; 5^\circ; 10^\circ; 30^\circ)$	10.3	361	30	428	4
3 families, $\theta_{13} = 5^\circ$	15.1	797	3	666	0
3 families, $\theta_{13} = 10^\circ$	14.4	755	12	632	1

Table 1

Event rates for the $\nu_\mu \rightarrow \nu_\tau$ and $\bar{\nu}_e \rightarrow \bar{\nu}_\tau$ channels for 1 kton MECC detector, exposed to a 2×10^{20} ($\nu_\mu, \bar{\nu}_e$) flux for one year, for different values of θ_{14}, θ_{24} and θ_{34} in the (3+1) scheme. The other unknown angle, θ_{13} has been fixed to: $\theta_{13} = 5^\circ, 10^\circ$. The CP-violating phases are: $\delta_1 = \delta_2 = 0; \delta_3 = 90^\circ$. As a reference, rates at the 1.8 kton OPERA detector (exposed to the nominal CNGS beam intensity) and the expected event rates for 1 kton MECC detector in the case of the three-family model (i.e., for $\theta_{i4} = 0$ and maximal CP-violating phase δ) are also shown. In all cases, perfect efficiency is assumed.

than the ECC [116]. We consider, however, this to be the only reasonable choice that we can take at this preliminary stage of four-family neutrino detailed study at the Neutrino Factory (not to be compared with the order-of-magnitude estimations made in previous papers).

Also in this case, we have grouped events into 10 bins with $\Delta E_\nu = 5$ GeV constant energy resolution. Global 10% systematic errors have been considered throughout the numerical simulations for both the $\nu_e \rightarrow \nu_\tau$ and the $\nu_\mu \rightarrow \nu_\tau$ signals.

In Tab. 1 we show the expected number of τ^- from $\nu_\mu \rightarrow \nu_\tau$ and τ^+ from $\bar{\nu}_e \rightarrow \bar{\nu}_\tau$ for a 1 kton MECC detector with perfect efficiency, exposed to a 2×10^{20} ($\nu_\mu, \bar{\nu}_e$) flux for one year, for different values of $\theta_{13}, \theta_{14}, \theta_{24}$ and θ_{34} . The other parameters are: $\theta_{12} = 34^\circ; \theta_{23} = 45^\circ; \Delta m_{\text{sol}}^2 = 7.9 \times 10^{-5}$ eV²; $\Delta m_{\text{atm}}^2 = 2.4 \times 10^{-3}$ eV² and $\Delta m_{\text{SBL}}^2 = 1$ eV² (all mass differences are taken to be positive). Eventually, phases have been fixed to: $\delta_1 = \delta_2 = 0; \delta_3 = 90^\circ$. For comparison, the rates at the CNGS (for the

nominal CNGS flux, of 4.5×10^{19} pot/year, an active lead target mass of 1.8 kton and 5 years of data taking) and the expected number of events in the three-family model for a 1 kton MECC detector with perfect efficiency are also shown. We can see that the number of expected τ^- events at the 1 Kton MECC is $O(500)$ at both baselines, with some dependence on the different mixing angles. The fact that at both baselines we expect a similar number of events is a consequence of the convolution of the $\nu_\mu \rightarrow \nu_\tau$ oscillation probability with the $\nu_\tau N$ cross-section and the ν_μ neutrino flux: at the shortest baseline, the probability is maximal below 10 GeV; at the longest baseline, the maximum is located in the 30 GeV bin. The higher cross-section for this energy bin compensates for the decrease in the ν_μ neutrino flux, thus giving a similar number of τ 's in the detector.

Notice that we will not use the MECC section of the Hybrid-MIND detector to look for the golden $\nu_e \rightarrow \nu_\mu$ and the $\nu_\mu \rightarrow \nu_\mu$ disappearance signals. Both channels can be studied, though, at the price of an increase in the scanning load.

4 Sensitivity to $(3+1)$ sterile neutrinos at the Neutrino Factory

In this section we study the physics reach of the 50 GeV Neutrino Factory setup discussed in the previous section to $(3+1)$ -model sterile neutrinos. We will make use of all possible oscillation channels available at this setup, namely the golden channel $\nu_e \rightarrow \nu_\mu$ and the disappearance channel $\nu_\mu \rightarrow \nu_\mu$ using the MIND section of the detector; the silver channel $\nu_e \rightarrow \nu_\tau$ and the "discovery channel" $\nu_\mu \rightarrow \nu_\tau$ using the MECC section of the detector.

We will first show in Sect. 4.1 how the golden and silver channels ($\nu_e \rightarrow \nu_\mu, \nu_\tau$) might cooperate to put a strong bound to the four-family model θ_{13} in the $(\theta_{13}, \theta_{14})$ plane, extending the standard three-family θ_{13} sensitivity analysis. Then, in Sect. 4.2, we will make use of the ν_μ disappearance channel and of the "discovery channel" $\nu_\mu \rightarrow \nu_\tau$ to improve significantly the exclusion bounds for $(3+1)$ -sterile neutrinos in the $(\theta_{24}, \theta_{34})$ plane. Preliminary results for the combination of these two channels at a 50 GeV Neutrino Factory setup have been presented in Refs. [117,118]. In both Sects. 4.1 and 4.2 we will also compare our results with those that could be obtained using the 20 GeV ISS-inspired Neutrino Factory defined in Sect. 3.

Eventually, in Sect. 4.3, we will show the attainable precision in the simultaneous measurement of θ_{34} and of the CP-violating phase δ_3 , in the case a positive signal for sterile neutrinos is found and both active-sterile mixing angles θ_{24} and θ_{34} are not exceedingly small.

4.1 Sensitivity to $(\theta_{13}, \theta_{14})$

The sensitivity is defined as follows: we first compute the expected number of events for $\nu_e \rightarrow \nu_\mu$ and $\nu_e \rightarrow \nu_\tau$ oscillations in the three-family model for the input value $\theta_{13}^{3\text{fam}} = 0$ (being $\theta_{13}^{3\text{fam}}$ the mixing angle in the three-family model). We then compute the expected number of events in the $(\theta_{13}^{4\text{fam}}, \theta_{14})$ -plane for the same oscillation channels, albeit in the four-family model (being $\theta_{13}^{4\text{fam}}$ the mixing angle in the four-family model). The $\Delta\chi^2$, computed with respect to the three-family "true" value, is eventually evaluated. The contour for which the 2 d.o.f.'s $\Delta\chi^2$ is $\Delta\chi^2 = 4.61$ defines, then, the region of the parameter space of the (3+1)-sterile neutrino model that is non-compatible at 90% CL with the input three-family data (to the right of the contour line) and the region that it is still allowed (to the left of the line) at this CL.

The minimum of the χ^2 is computed as follows:

$$\Delta\chi^2 = \min_{\text{marg par}} \left(\sum_j [N_j(4\text{fam}) + B_j(4\text{fam}) - N_j(3\text{fam}) - B_j(3\text{fam})]^2 / \sigma_j^2 \right), \quad (9)$$

where the minimization procedure is computed varying the parameters to be marginalized over (that can be different for different plots), and j runs over the different signals: the golden and silver channels, divided into 10 energy bins, for the two baselines and for the two possible stored muon polarities. B_j is the background correspondent to the j -signal, either in the three- or four-family model. Notice that we have minimized the χ^2 for each baseline, separately, and in the analysis combining the two baselines, we have minimized the sum of χ^2 for each baseline. The variance is defined as:

$$\sigma_j^2 = N_j(3\text{fam}) + B_j(3\text{fam}) + [f_j N_j(3\text{fam})]^2 + [f_j B_j(3\text{fam})]^2, \quad (10)$$

where f_j is the global systematic error on the j -channel: 2% for the golden channel and 10% for the silver channel, irrespectively of the energy bin, of the baseline and of the stored muon polarity. Notice that we can use the Gaussian expression for the χ^2 throughout our numerical simulation, with the possible exception of the silver channel data at the longest baseline, for which a Poissonian expression could be more appropriate due to the extremely low statistics (as it can be seen from Tab. 1). However, as it will be shown in the following discussion on the results, the impact of the silver channel at that baseline is negligible.

In the numerical analysis, the following parameters in common between three- and four-family models have been kept fixed to their central values⁶: $\theta_{12} = 34^\circ$, $\theta_{23} = 45^\circ$; $\Delta m_{\text{sol}}^2 = 7.9 \times 10^{-5} \text{ eV}^2$, $\Delta m_{31}^2 = 2.4 \times 10^{-3} \text{ eV}^2$; $\delta_2 = \delta = 0$ (where δ is the three-family CP-violating phase). The following two parameters specific to the four-family model have been also kept fixed: $\Delta m_{\text{SBL}}^2 = 1 \text{ eV}^2$ and $\delta_1 = 0$. Eventually, we have marginalized

⁶ We will not introduce any label to distinguish these parameters between three- and four-family models.

over $\theta_{24} \in [0, 12^\circ]$ and $\theta_{34} \in [0, 35^\circ]$. Matter effects have been included considering a constant matter density $\rho = 3.4 \text{ g/cm}^3$ for the shortest baseline and $\rho = 4.3 \text{ g/cm}^3$ for the longest one, computed averaging over the density profile in the PREM [85] along the neutrino path. We have checked that marginalization over a 10% matter density uncertainty does not modify our results.

Our results using the golden and silver channels are shown in Fig. 3, where the sensitivity to (3+1)-sterile neutrinos in the $(\theta_{13}, \theta_{14})$ -plane at 90% CL are presented. Results for the two baselines are shown both separately and summed: blue lines stand for the shortest baseline data; red lines stand for the longest baseline data; green lines stand for the sum of the two baselines. Eventually, solid lines stand for golden channel data, only, whereas dashed lines stand for the sum of golden and silver channels data. In this figure, the four-family CP-violating phase δ_3 has been fixed to four representative values: $\delta_3 = 0, 90^\circ, 180^\circ$ and 270° .

First of all, we can see from all panels that a rather good sensitivity to θ_{13}^{4fam} can be obtained using the 50 GeV Neutrino Factory setup, in the range $\sin^2 2\theta_{13}^{4fam} \leq [10^{-5}, 10^{-4}]$. The longest baseline outperforms the shortest one, with the exception of the top left panel where we can see that for vanishing δ_3 the shortest baseline performs slightly better and it is able to exclude values of θ_{13}^{4fam} down to $\sin^2 2\theta_{13}^{4fam} \leq 10^{-5}$. Some losses of θ_{13}^{4fam} -sensitivity for specific values of θ_{14} can be seen at the shortest baseline for $\delta_3 = 90^\circ, 180^\circ$, surely a consequence of some degeneracy in the oscillation probability. This is confirmed by looking at the effect of the inclusion of the silver channel. We can see both in the top right and bottom left panels that adding the silver channels data to the golden channel ones (dashed lines) either removes completely or reduces the sensitivity loss, smoothing the θ_{13}^{4fam} -sensitivity. This is the same effect that was observed in three-family analyses in the $(\theta_{13}^{3fam}, \delta)$ plane, where the so-called "intrinsic degeneracies" [68] were solved combining golden and silver channel data due to the different correlation between θ_{13}^{3fam} and δ in the oscillation probabilities. The similar behavior suggests, thus, that some parametric degeneracy, present at the shortest baseline and causing the θ_{13}^{4fam} -sensitivity loss has been solved by the inclusion of silver channel data. On the other hand, no effect whatsoever of the silver channel can be observed at the longest baseline, for any value of δ_3 . This is probably a consequence of a less severe degeneracy problem at this baseline and, clearly, of the extremely poor silver channel statistics at $L = 7500 \text{ km}$ from the source, as it can be seen from Tab. 1. Notice also that the θ_{13}^{4fam} -sensitivity at both baselines is only marginally dependent on θ_{14} , for very small values of the latter⁷, or for large θ_{14} at the longest baseline for $\delta_3 \neq 0$.

The combination of the two baselines gives, for all values of δ_3 , a smooth θ_{13}^{4fam} -

⁷ Using the four-family expressions for the oscillation probabilities in vacuum shown in Ref. [59], it can be seen that, for vanishing θ_{14} and θ_{24} , the four-family mixing angle θ_{13}^{4fam} maps into the three-family one, θ_{13}^{3fam} . On the other hand, for non-vanishing θ_{14} , the four-family parameter is expected to be slightly smaller than the three-family one.

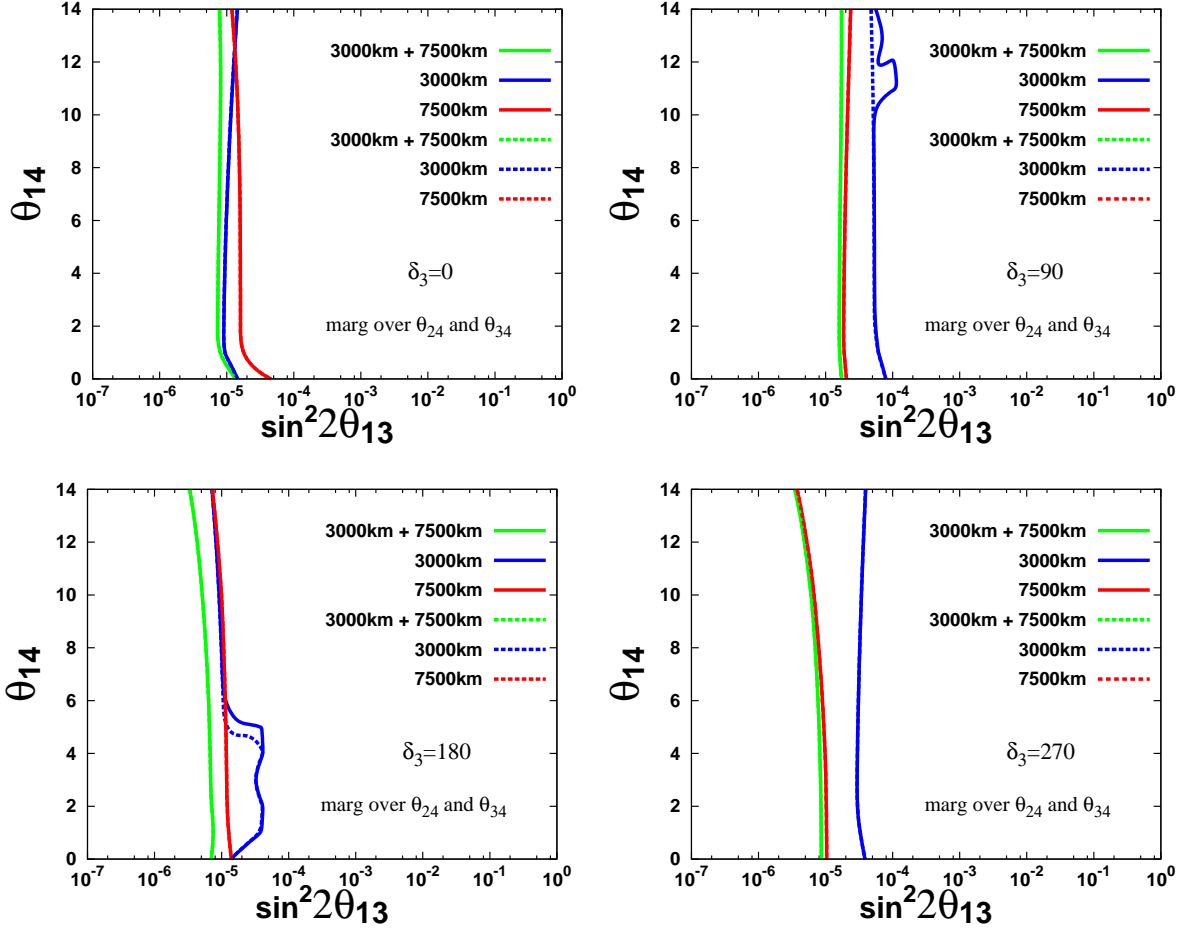


Fig. 3. Sensitivity limit at 90% CL in the $(\theta_{13}, \theta_{14})$ plane. The solid lines refer to the golden channel results, only. Dashed lines stand for the sum of golden and silver channel results. The colors are: blue for $L = 3000$ km; red for $L = 7500$ km; green for the combination of the two baselines. The four panels represent our results for: $\delta_3 = 0$ (top left); $\delta_3 = 90^\circ$ (top right); $\delta_3 = 180^\circ$ (bottom left); $\delta_3 = 270^\circ$ (bottom right).

sensitivity (showing that possible degeneracies at the shortest baseline can be solved by adding the second baseline and no silver channel, also, as it was the case in the three-family analysis) with only a marginal θ_{14} modulation.

We eventually compare the results obtained using the 50 GeV Neutrino Factory setup, Fig. 4(left), with those that can be achieved using the 20 GeV Neutrino Factory ISS-inspired setup, Fig. 4(right). As before, solid lines stand for golden channel data, only, whereas dashed lines stand for the combination of golden and silver channel data. Blue lines stand for the shortest baseline (3000 km or 4000 km); red lines for the longest baseline (7500 km in both setups); green lines for the combination of the two. In addition to θ_{24} and θ_{34} , we have marginalized over δ_3 , $\delta_3 \in [0, 360^\circ]$, also. The rest of the parameters have been kept fixed to the values given above.

The shortest baseline at the 20 GeV ISS-inspired setup (blue solid line in the left panel)

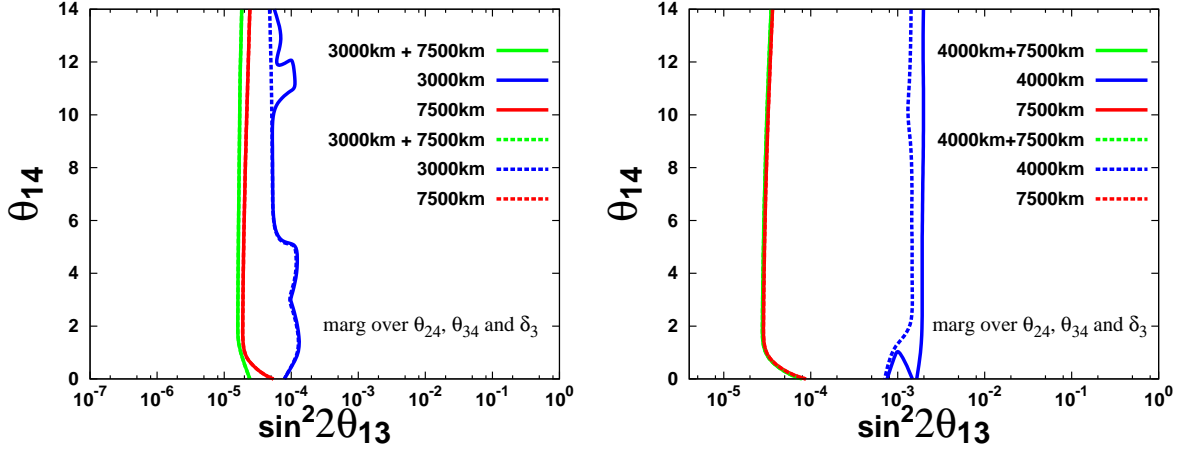


Fig. 4. Sensitivity limit at 90% CL in the $(\theta_{13}, \theta_{14})$ plane, marginalizing over θ_{24}, θ_{34} and δ_3 . The solid lines refer to the golden channel results, only. Dashed lines stand for the sum of golden and silver channel results. The colors are: blue for the shortest baseline; red for longest baseline; green for the combination of the two baselines. Left panel: 50 GeV Neutrino Factory; Right panel: 20 GeV Neutrino Factory.

has a rather poor θ_{13}^{4fam} -sensitivity, $\sin^2 2\theta_{13}^{4fam} \geq 2 \times 10^{-3}$ for any value of θ_{14} . For this particular case, the effect of the inclusion of the silver channel data is significant, as we can see from the blue dashed line. Although at 20 GeV the $\nu_\tau N$ cross-section is below $0.3 \times E_\nu \times 10^{-42} \text{ m}^2 \text{ GeV}^{-1}$, the collected statistics for the silver channel for $\theta_{13}^{4fam} \geq 2^\circ$ is sufficient to solve the sensitivity loss at the shortest baseline when added to golden channel data. The shortest baseline at the 50 GeV setup performs much better, with $\sin^2 2\theta_{13}^{4fam} \geq 2 \times 10^{-4}$ for any value of θ_{14} . On the other hand, the sensitivity at the longest baseline is substantially identical between the two setups, and in both cases much greater than at the shortest baseline. A non-vanishing four-family θ_{13}^{4fam} mixing angle can thus be excluded above $\sin^2 2\theta_{13}^{4fam} \geq 2.5 \times 10^{-5}$ for $\theta_{14} \geq 1^\circ$ and for any value of δ_3 , when the two baselines are combined.

4.2 Sensitivity to $(\theta_{24}, \theta_{34})$

The sensitivity is defined as in the previous section: we first compute the expected number of events for $\nu_\mu \rightarrow \nu_\mu$ and $\nu_\mu \rightarrow \nu_\tau$ oscillations in the three-family model; we then compute the expected number of events in the $(\theta_{24}, \theta_{34})$ -plane for the same oscillation channels in the four-family model. The $\Delta\chi^2$, computed with respect to the three-family "true" value, is eventually evaluated. The contour for which the 2 d.o.f.'s $\Delta\chi^2$ is $\Delta\chi^2 = 4.61$ defines, then, the region of the parameter space of the (3+1)-sterile neutrino model that is non-compatible at 90% CL with the input three-family data (above and to the right of the contour line) and the region that it is still allowed (below and to the left of the line).

The minimum of the χ^2 is computed as in Sect. 4.1:

$$\Delta\chi^2 = \min_{\text{marg par}} \left(\sum_j [N_j(4\text{fam}) + B_j(4\text{fam}) - N_j(3\text{fam}) - B_j(3\text{fam})]^2 / \sigma_j^2 \right) \quad (11)$$

where the minimization procedure is computed varying the parameters to be marginalized over (that can be different for different plots), and j runs over the different signals: the ν_μ disappearance and the $\nu_\mu \rightarrow \nu_\tau$ discovery channels, divided into 10 energy bins, for the two baselines and for the two possible stored muon polarities. B_j is the background correspondent to the j -signal, either in the three- or four-family model. Notice that we have minimized the χ^2 for each baseline, separately, and in the analysis combining the two baselines, we have minimized the sum of χ^2 for each baseline. The variance is defined as:

$$\sigma_j^2 = N_j(3\text{fam}) + B_j(3\text{fam}) + [f_j N_j(3\text{fam})]^2 + [f_j B_j(3\text{fam})]^2 \quad (12)$$

where f_j is the global systematic error on the j -channel: 5% for the ν_μ disappearance channel and 10% for the discovery channel, irrespectively of the energy bin, of the baseline and of the stored muon polarity.

In the numerical analysis, the central values of the following parameters in common between three- and four-family models are: $\theta_{12} = 34^\circ$, $\theta_{13} = 0$, $\theta_{23} = 45^\circ$; $\Delta m_{\text{sol}}^2 = 7.9 \times 10^{-5} \text{ eV}^2$, $\Delta m_{31}^2 = 2.4 \times 10^{-3} \text{ eV}^2$; $\delta_2 = \delta = 0$ (where δ is the three-family CP-violating phase). The central values for the following three parameters specific to the four-family model are: $\Delta m_{\text{SBL}}^2 = 1 \text{ eV}^2$, $\theta_{14} = 0$ and $\delta_1 = 0$. Matter effects have been included considering a constant matter density $\rho = 3.4 \text{ g/cm}^3$ for the shortest baseline and $\rho = 4.3 \text{ g/cm}^3$ for the longest one, computed averaging over the density profile in the PREM [85] along the neutrino path. We have checked that marginalization over a 10% matter density uncertainty does not modify our results.

The sensitivity to (3+1)-sterile neutrinos at the 90% CL in the $(\theta_{24}, \theta_{34})$ -plane for the 50 GeV Neutrino Factory setup is shown in Figs. 5,6 and 7. In these figures, we have studied how the marginalization over θ_{23} , Δm_{31}^2 and δ_3 modify our results by varying them separately or together in the ranges $\theta_{23} \in [40^\circ, 50^\circ]$, $\Delta m_{31}^2 \in [2.0, 2.8] \times 10^{-3} \text{ eV}^2$ and $\delta_3 \in [0, 360^\circ]$. We have also checked the impact of the marginalization over all the other parameters (otherwise fixed to their central values, given above), by studying them one by one in combination with θ_{23} , Δm_{31}^2 and δ_3 . The considered marginalization ranges are: $\theta_{12} \in [30^\circ, 36^\circ]$; $\theta_{13} \in [0, 10^\circ]$; $\theta_{14} \in [0, 10^\circ]$; $\Delta m_{21}^2 \in [7.0, 8.3] \times 10^{-5} \text{ eV}^2$; $\delta_1 \in [0, 360^\circ]$ and $\delta_2 \in [0, 360^\circ]$. We have found that none of these parameters modify significantly our results, contrary to the case of θ_{23} , Δm_{31}^2 and δ_3 . Eventually, we have checked that changing the sign of Δm_{31}^2 does not modify our results, either.

First of all, in Fig. 5 we show the sensitivity limit at 90% CL to θ_{24} and θ_{34} , for fixed Δm_{31}^2 and $\delta_3 = 0$, whilst marginalizing over θ_{23} in the range $\theta_{23} \in [40^\circ, 50^\circ]$. Notice that the considered allowed range for θ_{23} is a bit smaller than its present allowed range from the three-family global analysis. The Neutrino Factory, however, has an enormous

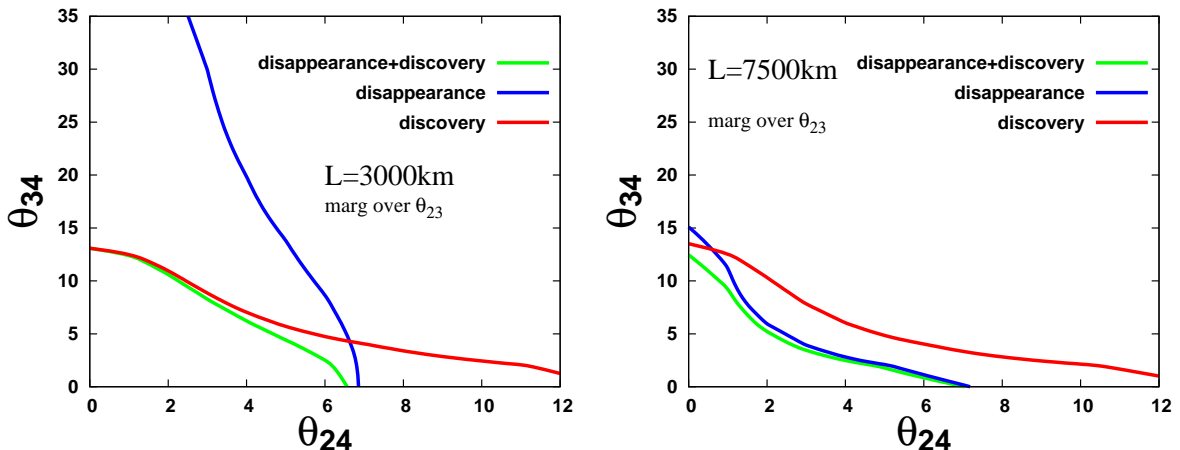


Fig. 5. Sensitivity limit at 90% CL to θ_{24} and θ_{34} , for fixed Δm_{31}^2 and $\delta_3 = 0$, whilst marginalizing over θ_{23} in the range $\theta_{23} \in [40^\circ, 50^\circ]$. Blue lines stands for the disappearance channel $\nu_\mu \rightarrow \nu_\mu$; red lines stand for the discovery channel $\nu_\mu \rightarrow \nu_\tau$; green lines stand for the combination of both. Left: $L = 3000$ km baseline, Right: $L = 7500$ km baseline.

potential for improving the measurement of the three-family atmospheric parameters through the ν_μ disappearance channel as it was shown, for example, in Ref. [108]. It is, therefore, absolutely reasonable to vary θ_{23} over a reduced range. In the two plots, blue lines stands for the $\nu_\mu \rightarrow \nu_\mu$ disappearance channel data; red lines stand for the $\nu_\mu \rightarrow \nu_\tau$ discovery channel data; green lines stand for the combination of both.

We discuss first the left panel of Fig. 5, that refers to the results at the shortest baseline, $L = 3000$ km. Notice that the disappearance channel has the strongest sensitivity to θ_{24} , that can be excluded above $\theta_{24} \sim 7^\circ$ for any value of θ_{34} (the leading dependence on θ_{24} arise at $O(\epsilon^4)$, as it will shown below). On the other hand, the $\nu_\mu \rightarrow \nu_\tau$ channel shows a strong correlation between θ_{24} and θ_{34} , with a bound on θ_{34} that is strongly dependent on the specific value of θ_{24} considered. This behavior can be understood by looking at eq. (7) in Sect. 2. First of all, the dominant term in $P_{\mu\tau}$ gives the ultimate sensitivity to θ_{34} for vanishing θ_{24} , $\theta_{34} \leq 15^\circ$. The strong correlation between the two mixing angles is induced by the subleading $O(\epsilon^3)$ term, proportional to $(A_n L) s_{24} s_{34} \cos \delta_3$ (since we are considering $\delta_3 = 0$ the term proportional to $\sin \delta_3$ vanishes). The same term induces some $(\theta_{24}, \theta_{34})$ -correlation in the disappearance channel, eq. (6), though significantly softer: a consequence of the different statistical significance of this term in appearance and disappearance channels. Eventually, the combination of the two channels gives a very good sensitivity to both mixing angles. A similar sensitivity is achieved at the longest baseline, $L = 7500$ km, whose results are shown in the right panel of Fig. 5. We can see comparing the red lines on both panels that the $\nu_\mu \rightarrow \nu_\tau$ channel sensitivity to $(\theta_{24}, \theta_{34})$ is substantially the same when changing baseline. This can be understood by looking at the expected number of events for this channel at the two baseline, Tab. 1. On the other hand, the blue line resembles now the red line: this is a consequence of the increased significance of the subleading term with respect to the dominant one in the disappearance channel due to larger matter effects at 7500 km.

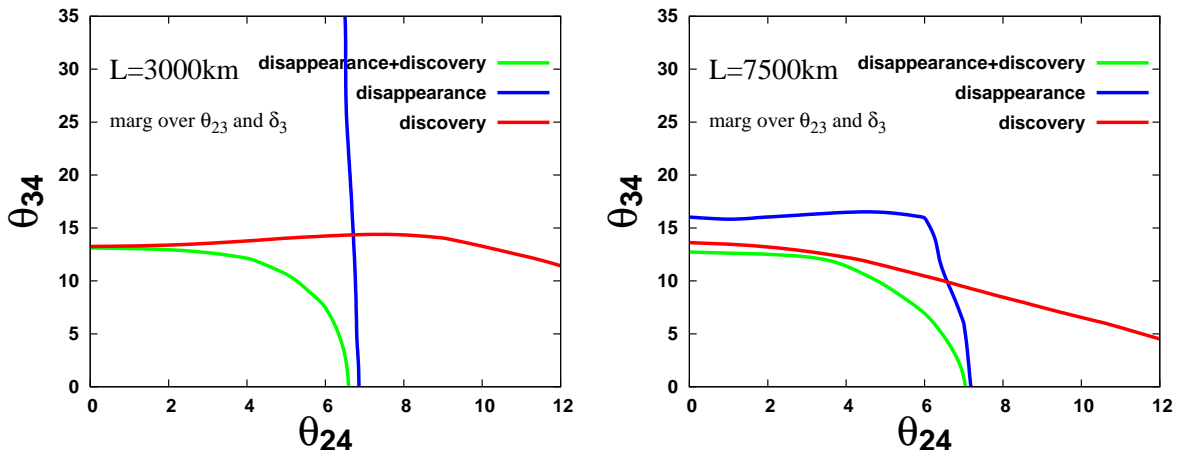


Fig. 6. Sensitivity limit at 90% CL to θ_{24} and θ_{34} , for fixed Δm_{31}^2 , whilst marginalizing over θ_{23} in the range $\theta_{23} \in [40^\circ, 50^\circ]$ and over the CP-violating phase $\delta_3 \in [0, 360^\circ]$. Blue lines stands for the disappearance channel $\nu_\mu \rightarrow \nu_\mu$; red lines stand for the discovery channel $\nu_\mu \rightarrow \nu_\tau$; green lines stand for the combination of both. Left: $L = 3000$ km baseline, Right: $L = 7500$ km baseline.

These behaviors are strongly modified if we marginalize over the CP-violating phase δ_3 , as it can be seen in Fig. 6 where we show the sensitivity limit at 90% CL to θ_{24} and θ_{34} , for fixed Δm_{31}^2 , whilst marginalizing over θ_{23} in the range $\theta_{23} \in [40^\circ, 50^\circ]$ and over δ_3 in the range $\delta_3 \in [0, 360^\circ]$. As before, blue lines stands for the $\nu_\mu \rightarrow \nu_\mu$ disappearance channel data; red lines stand for the $\nu_\mu \rightarrow \nu_\tau$ discovery channel data; green lines stand for the combination of both.

First of all, notice that the correlation between θ_{24} and θ_{34} in the disappearance channel sensitivity, induced by the $(A_n L) s_{24} s_{34} \cos \delta_3$ term in eq. (6), vanishes at the shortest baseline. This is a straightforward consequence of the marginalization over δ_3 . At this baseline, the disappearance channel shows no sensitivity whatsoever to θ_{34} . Something complementary also happens for the $\nu_\mu \rightarrow \nu_\tau$ sensitivity. The marginalization over δ_3 smoothens the impact of the two terms proportional to the combination $s_{24} s_{34}$, and the discovery channel sensitivity becomes a nearly horizontal line in the $(\theta_{24}, \theta_{34})$ -plane, thus signaling an effective loss of sensitivity to θ_{24} . Notice that some correlation between the two angles is still visible for large values of θ_{24} , $\theta_{24} \geq 8^\circ$. This effect increases at the longest baseline, where the $(A_n L)$ prefactor is enhanced by matter effects with respect to the $L = 3000$ km baseline. The correlation between the two angles shows up at smaller values of θ_{24} , $\theta_{24} \geq 4^\circ$. Some θ_{34} modulation of the straight line that we can see in the left panel is recovered for the disappearance channel sensitivity in the right panel. However, the most relevant feature that we can see for this channel at the longest baseline is a significant improvement in the sensitivity to θ_{34} for small values of θ_{24} : a horizontal line in the $(\theta_{24}, \theta_{34})$ -plane, much as it is the case for the $\nu_\mu \rightarrow \nu_\tau$ sensitivity.

The sensitivity of the disappearance channel to θ_{34} at the longest baseline arises at a higher order in the expansion that we have presented in eqs. (6,7). If we introduce

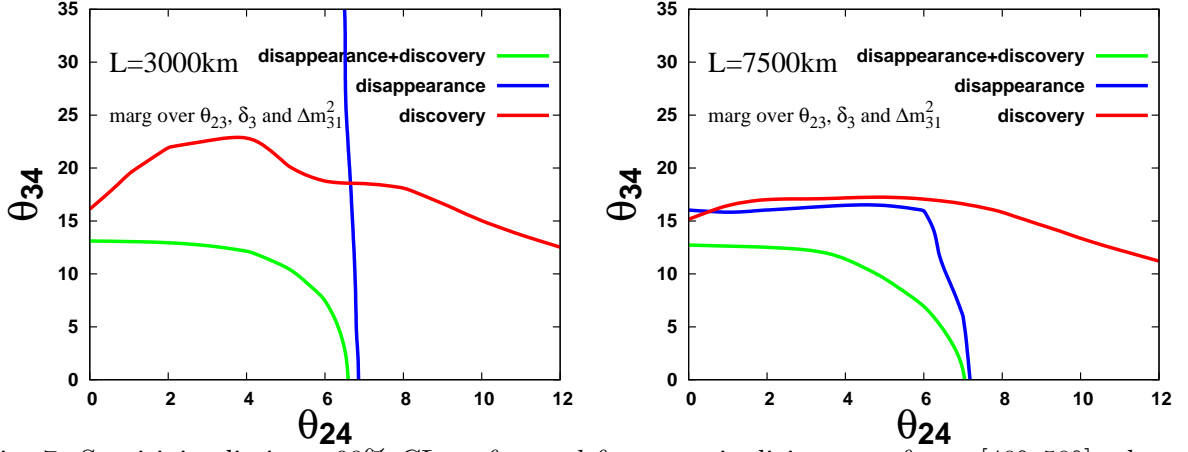


Fig. 7. Sensitivity limit at 90% CL to θ_{24} and θ_{34} , marginalizing over $\theta_{23} \in [40^\circ, 50^\circ]$, the CP-violating phase $\delta_3 \in [0, 360^\circ]$ and $\Delta m_{31}^2 \in [2.0, 2.8] \times 10^{-3} \text{eV}^2$. Blue lines stands for the disappearance channel $\nu_\mu \rightarrow \nu_\mu$; red lines stand for the discovery channel $\nu_\mu \rightarrow \nu_\tau$; green lines stand for the combination of both. Left: $L = 3000 \text{ km}$ baseline, Right: $L = 7500 \text{ km}$ baseline.

terms up to fourth order in ϵ (under the assumption $\theta_{13} = \theta_{14} = 0$, and taking into account the deviations from maximality of θ_{23}), we get:

$$P_{\mu\mu} = 1 - 2\theta_{24}^2 - \left[1 - 4(\delta\theta_{23})^2 - 2\theta_{24}^2 + \theta_{34}^2 \frac{A_n}{\Delta_{31}} \left(4\delta\theta_{23} - \theta_{34}^2 \frac{A_n}{\Delta_{31}} \right) \right] \sin^2 \frac{\Delta_{31}L}{2} - (A_n L) \left\{ 2\theta_{24} \theta_{34} \cos \delta_3 - \frac{\theta_{34}^2}{2} \left(4\delta\theta_{23} - \theta_{34}^2 \frac{A_n}{2\Delta_{31}} \right) \right\} \sin \Delta_{31}L + O(\epsilon^5), \quad (13)$$

$$P_{\mu\tau} = \left\{ 1 - 4(\delta\theta_{23})^2 - \theta_{24}^2 - \theta_{34}^2 \left[1 - \frac{\theta_{34}^2}{3} - \frac{A_n}{\Delta_{31}} \left(4\delta\theta_{23} - \theta_{34}^2 \frac{A_n}{\Delta_{31}} \right) \right] \right\} \sin^2 \frac{\Delta_{31}L}{2} + \left\{ \theta_{24} \theta_{34} \sin \delta_3 + (A_n L) \left[2\theta_{24} \theta_{34} \cos \delta_3 - \frac{\theta_{34}^2}{2} \left(4\delta\theta_{23} - \theta_{34}^2 \frac{A_n}{2\Delta_{31}} \right) \right] \right\} \sin \Delta_{31}L + O(\epsilon^5), \quad (14)$$

$$P_{\mu s} = 2\theta_{24}^2 + \left[\theta_{34}^2 \left(1 - \frac{\theta_{34}^2}{3} \right) - \theta_{24}^2 \right] \sin^2 \frac{\Delta_{31}L}{2} - \theta_{24} \theta_{34} \sin \delta_3 \sin \Delta_{31}L + O(\epsilon^5), \quad (15)$$

where A_n is the nucleon matter density parameter and $\delta\theta_{23} = \theta_{23} - \pi/4$.

Most of the θ_{34} -dependent terms in eq. (13) are proportional to the matter parameter ($A_n L$). This means that the impact of these terms will be more important at the longest baseline, than at the shortest one. This is the source of the θ_{34} -sensitivity in the disappearance channel that we observe at $L = 7500 \text{ km}$. On the other hand, the

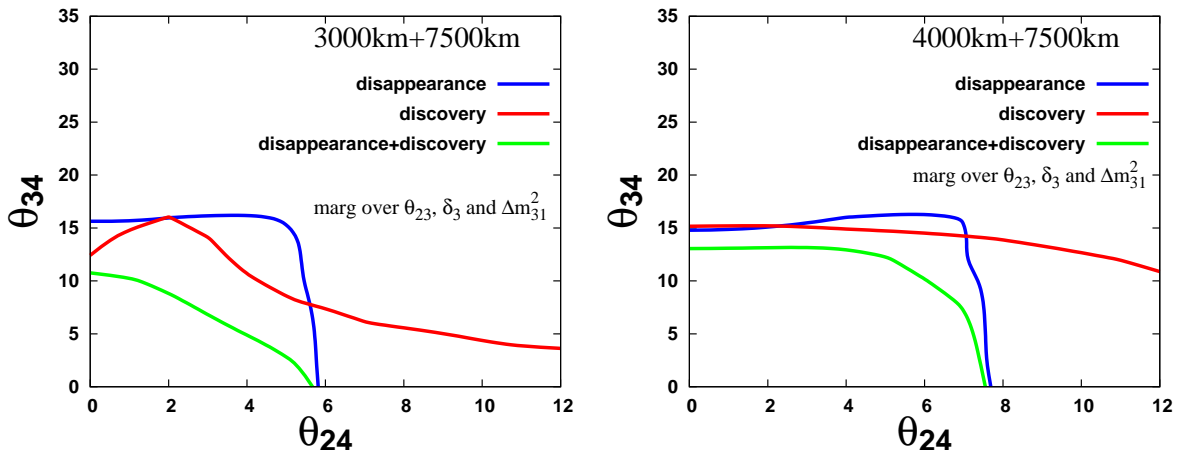


Fig. 8. Sensitivity limit at 90% CL to θ_{24} and θ_{34} , marginalizing over $\theta_{23} \in [40^\circ, 50^\circ]$, the CP-violating phase $\delta_3 \in [0, 360^\circ]$ and $\Delta m_{31}^2 \in [2.0, 2.8] \times 10^{-3} \text{eV}^2$, for the combination of the two baselines. Blue lines stands for the disappearance channel $\nu_\mu \rightarrow \nu_\mu$; red lines stand for the discovery channel $\nu_\mu \rightarrow \nu_\tau$; green lines stand for the combination of both. Left panel: 50 GeV Neutrino Factory; Right panel: 20 GeV Neutrino Factory.

θ_{24} -sensitivity arises from the θ_{24}^2 term at $O(\epsilon^4)$ in eq. (13).

We study, then, the effect of the marginalization over the atmospheric mass difference, Δm_{31}^2 . The results are shown in Fig. 7, where we present the sensitivity limit at 90% CL to θ_{24} and θ_{34} , whilst marginalizing over θ_{23} in the range $\theta_{23} \in [40^\circ, 50^\circ]$, over δ_3 in the range $\delta_3 \in [0, 360^\circ]$ and over Δm_{31}^2 in the range $\Delta m_{31}^2 \in [2.0, 2.8] \times 10^{-3} \text{eV}^2$. As before, blue lines stands for the $\nu_\mu \rightarrow \nu_\mu$ disappearance channel data; red lines stand for the $\nu_\mu \rightarrow \nu_\tau$ discovery channel data; green lines stand for the combination of both.

Comparing Figs. 6 and 7 we can see that the impact of the marginalization over the atmospheric mass difference on the disappearance channel sensitivity (blue lines) is negligible at both baselines. On the other hand, we can see a significant loss of sensitivity to θ_{34} in the $\nu_\mu \rightarrow \nu_\tau$ data (red lines) for $\theta_{24} \leq 6^\circ$ at the shortest baseline. This effect is a consequence of the complicated interplay between terms in the first and second lines of eq. (14). The cancellation disappears at the longest baseline, pointing out that the effect only occurs when $(A_n L)$ -proportional matter-dependent terms are small.

At the longest baseline, the ν_μ disappearance channel sensitivity dominates over the $\nu_\mu \rightarrow \nu_\tau$ one both for θ_{24} and θ_{34} . The combination of the two, however, is extremely effective and gives a very good sensitivity limit in both parameters.

We eventually compare the 90% CL $(\theta_{24}, \theta_{34})$ -sensitivity that can be obtained using the 50 GeV Neutrino Factory setup, Fig. 8(left), with the one that can be achieved using the 20 GeV Neutrino Factory ISS-inspired setup, Fig. 8(right). As before, blue lines stand for ν_μ disappearance channel data; red lines for the $\nu_\mu \rightarrow \nu_\tau$ discovery channel data; and green lines for the combination of both channels. Data for the two baselines are always summed. In these plots, we have marginalized over $\theta_{23} \in [40^\circ, 50^\circ]$,

$\delta_3 \in [0, 360^\circ]$ and $\Delta m_{31}^2 \in [2.0, 2.8] \times 10^{-3} \text{eV}^2$. The rest of the parameters have been kept fixed to the values given previously.

First of all, we can see by comparing blue lines (the disappearance channel data) between Fig. 8(left) and Fig. 8(right) that, although the sensitivity to θ_{34} at the two setups is similar, the sensitivity to θ_{24} at the 20 GeV Neutrino Factory is significantly worse than at the 50 GeV one, with $\theta_{24} \leq 8^\circ$ compared with $\theta_{24} \leq 6^\circ$. The sensitivity to $(\theta_{24}, \theta_{34})$ using the discovery channel (red lines) is also consistently better at the 50 GeV Neutrino Factory than at the 20 GeV one, a straightforward consequence of the higher statistics due to the higher $\nu_\tau N$ cross-section. For this reason, contrary to the case of the sensitivity to θ_{13}^{4fam} , for which we have shown in Fig. 4 that the two different Neutrino Factory setups have similar performances, the 50 GeV Neutrino Factory severely outperforms the 20 GeV ISS-inspired one when the two channels are combined, as it can be seen comparing the green lines in Fig. 8.

Our final conclusion is that, using the 50 GeV Neutrino Factory setup proposed in Sect. 3, an ultimate sensitivity to $\theta_{34} \leq 10^\circ$ for vanishing θ_{24} at 90% CL can be achieved combining the ν_μ disappearance channel and the $\nu_\mu \rightarrow \nu_\tau$ discovery channel at the two baselines, $L = 3000$ km and $L = 7500$ km. At the same time, we obtain an ultimate sensitivity to $\theta_{24} \leq 6^\circ$ for vanishing θ_{34} at 90% CL. For the 20 GeV ISS-inspired setup, the ultimate sensitivity limits are $\theta_{34} \leq 13^\circ$ and $\theta_{24} \leq 7.5^\circ$, respectively.

4.3 A CP-violating sterile neutrino signal

In the previous sections we have considered the case of a null result for sterile neutrino searches at the Neutrino Factory after 4 years running for both muon polarities, showing exclusion plots both in the $(\theta_{13}^{4fam}, \theta_{14})$ - and in the $(\theta_{24}, \theta_{34})$ -planes. However, due to the impressive statistics achievable at the Neutrino Factory, it could well be possible that a positive signal is found (if sterile neutrinos with $O(1\text{eV}^2)$ mass difference with respect to active ones do exist). In this case, we can try to measure some of the mixing angles and, more importantly, some of the CP-violating phases.

We will present in this section a first analysis of the precision achievable in our setup in the simultaneous measurement of mixing angles and CP-violating phases, focusing on θ_{34} and on the CP-violating phase δ_3 . Notice that each of the three possible CP-violating signals in a four-family model is related to a different Jarlskog invariant, proportional to a different combination of the mixing angles. We will consider in this section only the $\sin \delta_3$ -dependent one. The relevant Jarlskog invariant for this signal is, in our parametrization, proportional to the combination $\sin 2\theta_{23}s_{24}s_{34} \sin \delta_3 \simeq s_{24}s_{34} \sin \delta_3$. Clearly, a measurement of δ_3 is possible only if both θ_{24} and θ_{34} are simultaneously non-vanishing. We will consider in our analysis several fixed values of θ_{24} and draw 90% CL contours in the (θ_{34}, δ_3) -plane for particular input pairs $(\bar{\theta}_{34}, \bar{\delta}_3)$.

The measurement of these two parameters is achieved combining data from the ν_μ disappearance channel and the $\nu_\mu \rightarrow \nu_\tau$ discovery channel. This analysis, of course, does

not pretend to be as exhaustive as those that have been presented in the framework of the three-family model. In particular, we will not address within a comprehensive approach the problem of degeneracies in four-family models. Notice that this problem, extremely severe in the three-family oscillation studies at the Neutrino Factory (see, for example, Refs. [68]-[107] and Ref. [119]), is expected to be even more complicated in a four-neutrino model. In the particular case of the δ_3 -dependent CP-violating signal, that can be extracted using the $\nu_\mu \rightarrow \nu_\mu$ and $\nu_\mu \rightarrow \nu_\tau$ channels, we do expect to observe degeneracies due to the (θ_{34}, δ_3) -correlation (the so-called "intrinsic degeneracies", [68]); those dependent on the wrong reconstruction of the neutrino mass hierarchy (known as "sign degeneracies", [69]); and, eventually, those dependent on a wrong reconstruction of the "atmospheric" mixing angle θ_{23} octant (known as "octant degeneracies", [106]).

We show in Fig. 9 the 2 d.o.f.'s 99 %CL contours for the simultaneous measurement of θ_{34} and δ_3 using the combined data from the disappearance and the "discovery" channels for two representative values of θ_{24} : $\theta_{24} = 3^\circ$ (left panel) and $\theta_{24} = 5^\circ$ (right panel). Blue dot-dashed lines stand for the $L = 3000$ km baseline; red dashed lines stand for the $L = 7500$ km baseline; black solid lines stand for the combination of both baselines.

The contours in the (θ_{34}, δ_3) -plane have been obtained as follows: we have first computed the expected number of events for $\nu_\mu \rightarrow \nu_\mu$ and $\nu_\mu \rightarrow \nu_\tau$ oscillations in the four-family model for a particular choice of the relevant parameters, $\theta_{24} = \bar{\theta}_{24}$, $\theta_{34} = \bar{\theta}_{34}$ and $\delta_3 = \bar{\delta}_3$. We have then computed the expected number of events in the (θ_{34}, δ_3) -plane for the same oscillation channels in the four-family model, varying $\theta_{34} \in [0, 35^\circ]$ and $\delta_3 \in [0, 360^\circ]$. The $\Delta\chi^2$ is then computed as follows:

$$\Delta\chi^2 = \left(\sum_j \left[N_j(\bar{\theta}_{24}, \theta_{34}, \delta_3) - N_j(\bar{\theta}_{24}, \bar{\theta}_{34}, \bar{\delta}_3) \right]^2 / \sigma_j^2 \right) \quad (16)$$

where the minimum of the χ^2 is, trivially, obtained for $\theta_{34} = \bar{\theta}_{34}$; $\delta_3 = \bar{\delta}_3$. As before, j runs over the different signals: the ν_μ disappearance and the $\nu_\mu \rightarrow \nu_\tau$ discovery channels data, divided into 10 energy bins, for the two baselines and the two possible stored muons polarities. The variance is defined as before:

$$\sigma_j^2 = N_j(4\text{fam}) + B_j(4\text{fam}) + [f_j N_j(4\text{fam})]^2 + [f_j B_j(4\text{fam})]^2 \quad (17)$$

where f_j is the global systematic error on the j -channel: 5% for the ν_μ disappearance channel and 10% for the discovery channel, irrespectively of the energy bin, of the baseline and of the stored muon polarity. The region in the (θ_{34}, δ_3) -plane compatible with the input values $(\bar{\theta}_{34}, \bar{\delta}_3)$ at the 2 d.o.f.'s 99% CL is eventually defined by drawing the contour line corresponding to $\Delta\chi^2 = 9.21$.

In the numerical analysis, the following parameters in the four-family model have been kept fixed to their central values: $\theta_{12} = 34^\circ$, $\theta_{13} = 0$; $\Delta m_{\text{sol}}^2 = 7.9 \times 10^{-5}$ eV²; $\Delta m_{31}^2 = \Delta m_{\text{atm}}^2 = 2.4 \times 10^{-3}$ eV²; $\delta_1 = \delta_2 = 0$. Eventually, $\Delta m_{\text{SBL}}^2 = 1$ eV² and $\theta_{14} = 0^\circ$. For simplicity, we have fixed $\theta_{23} = 45^\circ$. We do not expect any "octant degeneracies", thus.

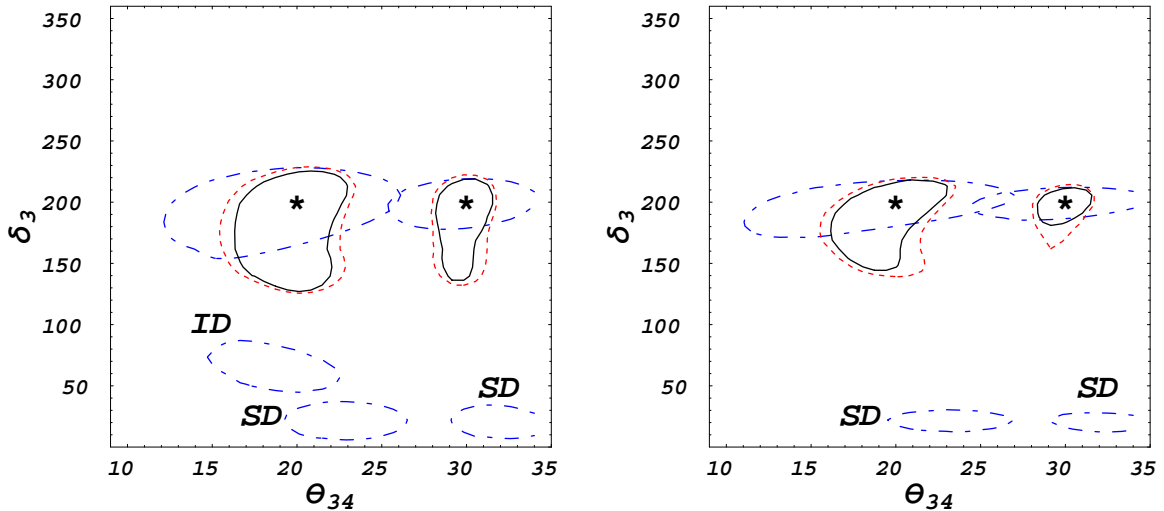


Fig. 9. 99% CL contours for the simultaneous measurement of θ_{34} and δ_3 using the combined data from the ν_μ disappearance and the $\nu_\mu \rightarrow \nu_\tau$ discovery channels. Two different values of θ_{24} have been considered: $\theta_{24} = 3^\circ$ (left panel); $\theta_{24} = 5^\circ$ (right panel). The input pairs $(\bar{\theta}_{34}, \bar{\delta}_3)$, marked by a star in the plots, are: $\bar{\theta}_{34} = 20^\circ, 30^\circ$; $\bar{\delta}_3 = 200^\circ$. In the plots, "ID" stands for "Intrinsic Degeneracy"; "SD" stands for "Sign Degeneracy". Blue dot-dashed lines represent the $L = 3000$ km baseline data; red dashed lines the $L = 7500$ km baseline data; black solid lines stand for the combination of both baselines.

The input values that we have studied to illustrate the discovery potential of our setup are: $\bar{\theta}_{34} = 20^\circ, 30^\circ$; $\bar{\delta}_3 = 200^\circ$ (we have analyzed also other possible input values for $\bar{\delta}_3$, obtaining similar results). Matter effects have been included considering, as always, a constant matter density $\rho = 3.4$ g/cm³ for the shortest baseline and $\rho = 4.3$ g/cm³ for the longest one, computed averaging over the density profile in the PREM [85] along the neutrino path.

First of all, we can see in Fig. 9(right), corresponding to $\bar{\theta}_{24} = 5^\circ$, how using the shortest baseline data (blue dot-dashed lines) the achievable precision on δ_3 is rather good for both θ_{34} input values: the error in δ_3 at the 99% CL is a few tens of degrees, at most. On the other hand, the shortest baseline data are clearly affected by sign degeneracies (labeled with "SD" in the plot). For this particular δ_3 input value the "sign clones" appear at $\delta_3^{\text{SD}} \sim 20^\circ$. The problem is solved, however, if we consider now the longest baseline data (red dashed lines). In this case, we can see that a rather good precision on θ_{34} is achievable, of the order of a few degrees. A poorer precision on δ_3 with respect to the shortest baseline data is obtained (some tens of degrees). Most important is that, at this baseline, no "sign clones" are present. The combination of the two baselines (black solid lines) shows no sign degeneracies.

In Fig. 9(left), corresponding to $\bar{\theta}_{24} = 3^\circ$, we can see that at the shortest baseline not only sign degeneracies are present, but also remnants of the intrinsic degeneracies (labeled with "ID") for $\bar{\theta}_{34} = 20^\circ$. Again, no degeneracies (neither sign nor intrinsic) can be seen at the longest baseline. The combination of the two baselines achieve a

rather good precision on θ_{34} , of the order of a few degrees, and some precision on δ_3 , discriminating clearly $\bar{\delta}_3 = 200^\circ$ from the vanishing δ_3 hypothesis.

5 Conclusions

We have studied the potential of a Neutrino Factory to search for signature of the (3+1)-scheme, where the largest mass squared difference Δm_{SBL}^2 can be any value larger than 0.1 eV^2 , as long as oscillations driven by Δm_{SBL}^2 are averaged for the range of the energy and the baseline at a Neutrino Factory. From the analytic expressions of the oscillation probabilities, we have seen that the disappearance channel $\nu_\mu \rightarrow \nu_\mu$ and the “*discovery channel*” $\nu_\mu \rightarrow \nu_\tau$ are extremely powerful in constraining the parameter space of the (3+1)-scheme.

We have performed a numerical analysis of the sensitivity to sterile neutrinos in two setups: (a) A Neutrino Factory with the muon energy $E_\mu = 50 \text{ GeV}$, 2×10^{20} useful muon decays per year per baseline, with two detectors located at $L = 3000 \text{ km}$ and $L = 7500 \text{ km}$ from the source, respectively; (b) The setup suggested in the final ISS Physics Report, i.e., a Neutrino Factory with $E_\mu = 20 \text{ GeV}$, 5×10^{20} useful muon decays per year per baseline, with two detectors located at $L = 4000 \text{ km}$ and $L = 7500 \text{ km}$ from the source, respectively. The two detectors are of the Hybrid-MIND type (50 kton MIND + 4 kton MECC). In both cases we have assumed data taking for 4 years for both muon polarities. We have carefully taken into account the relevant backgrounds, efficiencies and systematic errors and our analysis is, thus, much more detailed than in previous studies in the literature. Combining the disappearance and discovery channels, we have found that the 50 GeV (20 GeV) Neutrino Factory can constrain θ_{34} and θ_{24} down to 10° and 6° (13° and 7.5°), respectively, marginalizing over all other four-family parameters. The present results should be compared to the previous study [59] on the CNGS experiment, which cannot improve the present bound on θ_{24} and θ_{34} , if running at the nominal luminosity. The sensitivity to θ_{24} and θ_{34} of the 50 GeV Neutrino Factory setup proposed in this paper is better than the potential sensitivity of the CNGS experiment even if the CNGS beam intensity would be increased by a factor 10.

We have also looked at the sensitivity to θ_{13} , θ_{14} . In this case the golden $\nu_e \rightarrow \nu_\mu$ and silver channels $\nu_e \rightarrow \nu_\tau$ are powerful as in the case of the three flavor framework. While Neutrino Factories do not give any useful constraint on θ_{14} , they give quite a strong constraint on $\sin^2 2\theta_{13}$, down to 2×10^{-5} (3×10^{-5}) for the 50 GeV (20 GeV) case with a slight dependence on θ_{14} . In this analysis we found that the silver channel plays an important role in resolving parameter degeneracies at the shortest baseline particularly for the 20 GeV case. In the present work we did not assume any near detector, since the issue has not yet been studied much (see [120]). If we put a near detector, then we should be able to give a constraint on θ_{14} because the near detector will give us information on how much neutrino oscillations occur due to the largest mass squared difference Δm_{SBL}^2 . Further studies on the near detector will be necessary

to obtain quantitative results on θ_{14} .

On the other hand, in the case where we have a positive signal of the sterile neutrino mixing, we have found that we can measure the CP phase δ_3 by combining the disappearance and discovery channels at the two baselines, where information from the $L = 7500$ km baseline plays a dominant role in resolving parameter degeneracy. While our works contain some results on parameter degeneracy in the (3+1)-scheme, the problem on the general structure of parameter degeneracy in the four neutrino schemes is beyond the scope of the present paper and should be pursued in future.

Finally, we would like to stress that, while the discovery channel at a Neutrino Factory is not very useful for the measurements of the three flavor oscillation parameters, it is a very important channel to search for new physics beyond the standard scenario. The discovery channel at a Neutrino Factory deserves further studies.

Appendix

A Oscillation probabilities by the KTY formalism

To derive the expressions for the oscillation probabilities in matter, we use the KTY formalism which has been introduced in Ref. [61,62]⁸. The evolution equation of flavor eigenstates⁹ is:

$$i \frac{d}{dt} |\nu_\alpha\rangle = \mathcal{H}_{\alpha\beta} |\nu_\beta\rangle \equiv [U\mathcal{E}U^\dagger + \mathcal{A}]_{\alpha\beta} |\nu_\beta\rangle,$$

where

$$\begin{aligned} \mathcal{E} &= \text{diag}\left(0, \frac{\Delta m_{21}^2}{2E}, \frac{\Delta m_{31}^2}{2E}, \frac{\Delta m_{41}^2}{2E}\right) \equiv \text{diag}(0, \Delta_{21}, \Delta_{31}, \Delta_{41}), \\ \mathcal{A} &= \sqrt{2} G_F \text{diag}(n_e, 0, 0, n_n/2) \equiv \text{diag}(A_e, 0, 0, A_n), \end{aligned} \quad (\text{A.1})$$

$\Delta_{ij} = \Delta m_{ij}^2/2E$, and n_e and n_n are respectively the electron and neutron densities. In Eq. (A.1), we have subtracted from \mathcal{H} the term $E_1 \mathbf{1} = \sqrt{E^2 + m_1^2} \mathbf{1}$, which contributes only to the phase of the oscillation amplitude and therefore does not affect the probability. In the KTY formalism, the oscillation probabilities in matter assume the following form:

⁸ Another proof of the KTY formalism was given in Ref. [121,122] and it was extended to four neutrino schemes in Ref. [123].

⁹ Greek (Latin) indices label the flavor (mass) basis: $\alpha = e, \mu, \tau, s$ ($i = 1, 2, 3, 4$).

$$P_{\alpha\beta} = \delta_{\alpha\beta} - 4 \sum_{i<j} \text{Re}(\tilde{X}_i^{\alpha\beta} \tilde{X}_j^{\alpha\beta*}) \sin^2 \left(\frac{\Delta \tilde{E}_{ij} L}{2} \right) + 2 \sum_{i<j} \text{Im}(\tilde{X}_i^{\alpha\beta} \tilde{X}_j^{\alpha\beta*}) \sin(\Delta \tilde{E}_{ij} L), \quad (\text{A.2})$$

where $\Delta \tilde{E}_{ji} \equiv \tilde{E}_j - \tilde{E}_i$ and $\tilde{X}_j^{\alpha\beta} \equiv \tilde{U}_{\alpha j} \tilde{U}_{\beta j}^*$ ($j = 1, 2, 3, 4$). \tilde{E}_i and $\tilde{U}_{\alpha i}$ are the \mathcal{H} eigenvalues and the effective mixing matrix in matter, respectively, defined through

$$\mathcal{H} = \tilde{U} \text{diag}(\tilde{E}_j) \tilde{U}^\dagger.$$

The $\tilde{X}_j^{\alpha\beta}$ matrices can be expressed as follows:

$$\tilde{X}_j^{\alpha\beta} \equiv \sum_l (V^{-1})_{jl} [\mathcal{H}^{l-1}]_{\alpha\beta} = \sum_l (V^{-1})_{jl} \left[(U \mathcal{E} U^\dagger + \mathcal{A})^{l-1} \right]_{\alpha\beta}, \quad (\text{A.3})$$

where V is the Vandermonde matrix:

$$V = \begin{pmatrix} 1 & 1 & 1 & 1 \\ \tilde{E}_1 & \tilde{E}_2 & \tilde{E}_3 & \tilde{E}_4 \\ \tilde{E}_1^2 & \tilde{E}_2^2 & \tilde{E}_3^2 & \tilde{E}_4^2 \\ \tilde{E}_1^3 & \tilde{E}_2^3 & \tilde{E}_3^3 & \tilde{E}_4^3 \end{pmatrix},$$

whose determinant is $\prod_{i<j} \Delta \tilde{E}_{ji}$. The inverse of V can then be easily obtained as long as we know the eigenvalues \tilde{E}_j of the effective Hamiltonian in matter \mathcal{H} , expressed in terms of A_e , A_n and the vacuum parameters:

$$V^{-1} = \begin{pmatrix} \frac{1}{\Delta \tilde{E}_{21} \Delta \tilde{E}_{31} \Delta \tilde{E}_{41}} (\tilde{E}_2 \tilde{E}_3 \tilde{E}_4, -(\tilde{E}_2 \tilde{E}_3 + \tilde{E}_3 \tilde{E}_4 + \tilde{E}_4 \tilde{E}_2), \tilde{E}_2 + \tilde{E}_3 + \tilde{E}_4, -1) \\ \frac{-1}{\Delta \tilde{E}_{21} \Delta \tilde{E}_{32} \Delta \tilde{E}_{42}} (\tilde{E}_3 \tilde{E}_4 \tilde{E}_1, -(\tilde{E}_3 \tilde{E}_4 + \tilde{E}_4 \tilde{E}_1 + \tilde{E}_1 \tilde{E}_3), \tilde{E}_3 + \tilde{E}_4 + \tilde{E}_1, -1) \\ \frac{1}{\Delta \tilde{E}_{31} \Delta \tilde{E}_{32} \Delta \tilde{E}_{43}} (\tilde{E}_4 \tilde{E}_1 \tilde{E}_2, -(\tilde{E}_4 \tilde{E}_1 + \tilde{E}_1 \tilde{E}_2 + \tilde{E}_2 \tilde{E}_4), \tilde{E}_4 + \tilde{E}_1 + \tilde{E}_2, -1) \\ \frac{-1}{\Delta \tilde{E}_{41} \Delta \tilde{E}_{42} \Delta \tilde{E}_{43}} (\tilde{E}_1 \tilde{E}_2 \tilde{E}_3, -(\tilde{E}_1 \tilde{E}_2 + \tilde{E}_2 \tilde{E}_3 + \tilde{E}_3 \tilde{E}_1), \tilde{E}_1 + \tilde{E}_2 + \tilde{E}_3, -1) \end{pmatrix}. \quad (\text{A.4})$$

Within the KTY formalism, thus, we only need to compute the eigenvalues of \mathcal{H} to derive the oscillation probabilities in matter.

A possible drawback of this approach is that the physical understanding of the oscillation probabilities (i.e. the dependence on the vacuum mixing matrix parameters) is encoded in the explicit expressions for the \tilde{X} coefficients. To make contact with the parameters to be measured in a manageable way, we thus need to introduce some ap-

proximations in the computation of the eigenvalues \tilde{E}_i and of the corresponding matrices $\tilde{X}_i^{\alpha\beta}$. Now, considering the present constraints from [59] in the standard and sterile small parameters, we see that θ_{13}, θ_{14} and θ_{24} cannot be much larger than 10° while the third active-sterile mixing angle, θ_{34} , can be as large as $\theta_{34} \sim 35^\circ$. Notice also that the present constraint on the θ_{23} deviation from the maximal mixing, $\delta\theta_{23} \equiv \theta_{23} - \pi/4$, is of the same order as those on θ_{13}, θ_{14} and θ_{24} . On the other hand, the solar and atmospheric mass differences, $\Delta m_{\text{sol}}^2, \Delta m_{\text{atm}}^2$, are much smaller than Δm_{SBL}^2 . In what follows, therefore, we expand all the quantities in power of a small parameter ϵ , and keep terms of cubic order in ϵ , where the small parameter is defined by

$$\begin{aligned}\epsilon &\equiv s_{34} \sim \sqrt{s_{13}} \sim \sqrt{s_{14}} \sim \sqrt{s_{24}} \sim \sqrt{\delta\theta_{23}} \lesssim 4 \times 10^{-1}, \\ \eta_2 &\equiv \Delta m_{21}^2 / \Delta m_{41}^2 \lesssim 10^{-4}, \\ \eta_3 &\equiv \Delta m_{31}^2 / \Delta m_{41}^2 \lesssim 10^{-3}, \\ \eta_{e(n)} &\equiv A_{e(n)} / \Delta E_{41} \lesssim 10^{-3}.\end{aligned}$$

Notice that, to third order in ϵ , in the expansion in the probabilities we have neglected all terms proportional to $\eta_{e,n,3}$. Although this can be a rather rough approximation, as we have seen below, it is very useful in order to understand the different physics potential of the various oscillation channels. Thus we have the following probabilities to third order in ϵ :

$$\begin{aligned}P_{ee} &\sim 1 + \mathcal{O}(\epsilon^4), \\ P_{e\mu} &\sim P_{e\tau} \sim P_{es} \sim \mathcal{O}(\epsilon^4), \\ P_{\mu\mu} &= 1 - \sin^2 \frac{\Delta_{31}L}{2} - 2(A_n L) s_{24} s_{34} \cos \delta_3 \sin \Delta_{31}L + \mathcal{O}(\epsilon^4), \\ P_{\mu\tau} &= \left(1 - s_{34}^2\right) \sin^2 \frac{\Delta_{31}L}{2} + \{s_{24} s_{34} \sin \delta_3 + 2(A_n L) s_{24} s_{34} \cos \delta_3\} \sin \Delta_{31}L \\ &\quad + \mathcal{O}(\epsilon^4), \\ P_{\mu s} &= s_{34}^2 \sin^2 \frac{\Delta_{31}L}{2} - s_{24} s_{34} \sin \delta_3 \sin \Delta_{31}L + \mathcal{O}(\epsilon^4).\end{aligned}$$

As a final analytical contribution, we have calculated approximate probabilities associated to the channels under study, $P_{\mu\mu}$ and $P_{\mu\tau}$ (together with $P_{\mu s}$), up to fourth order in ϵ but neglecting θ_{13} and θ_{14} :

$$\begin{aligned}P_{\mu\mu} &= 1 - 2\theta_{24}^2 - \left[1 - 4(\delta\theta_{23})^2 - 2\theta_{24}^2 + \theta_{34}^2 \frac{A_n}{\Delta_{31}} \left(4\delta\theta_{23} - \theta_{34}^2 \frac{A_n}{\Delta_{31}}\right)\right] \sin^2 \frac{\Delta_{31}L}{2} \\ &\quad - (A_n L) \left\{2\theta_{24} \theta_{34} \cos \delta_3 - \frac{\theta_{34}^2}{2} \left(4\delta\theta_{23} - \theta_{34}^2 \frac{A_n}{2\Delta_{31}}\right)\right\} \sin \Delta_{31}L + \mathcal{O}(\epsilon^5),\end{aligned}$$

$$\begin{aligned}
P_{\mu\tau} = & \left\{ 1 - 4(\delta\theta_{23})^2 - \theta_{24}^2 - \theta_{34}^2 \left[1 - \frac{\theta_{34}^2}{3} - \frac{A_n}{\Delta_{31}} \left(4\delta\theta_{23} - \theta_{34}^2 \frac{A_n}{\Delta_{31}} \right) \right] \right\} \sin^2 \frac{\Delta_{31}L}{2} \\
& + \left\{ \theta_{24} \theta_{34} \sin \delta_3 + (A_n L) \left[2\theta_{24} \theta_{34} \cos \delta_3 - \frac{\theta_{34}^2}{2} \left(4\delta\theta_{23} - \theta_{34}^2 \frac{A_n}{2\Delta_{31}} \right) \right] \right\} \sin \Delta_{31}L \\
& + O(\epsilon^5),
\end{aligned}$$

$$\begin{aligned}
P_{\mu s} = & 2\theta_{24}^2 + \left[\theta_{34}^2 \left(1 - \frac{\theta_{34}^2}{3} \right) - \theta_{24}^2 \right] \sin^2 \frac{\Delta_{31}L}{2} - \theta_{24} \theta_{34} \sin \delta_3 \sin \Delta_{31}L \\
& + O(\epsilon^5).
\end{aligned}$$

Acknowledgements

We acknowledge H. Minakata for useful comments, P. Migliozzi for useful discussions, and P. Lipari and M. Lusignoli for discussions. The work has been partially supported by the JSPS-CSIC Bilateral Joint Projects (Japan-Spain), a Grant-in-Aid for Scientific Research of the Ministry of Education, Science and Culture of Japan, #19340062. K.F. thanks the support by the MEXT program "Support Program for Improving Graduate School Education"; J. L.-P. acknowledges partial financial support by the Ministry of Science and Innovation of Spain (MICINN) through an FPU grant, ref. AP2005-1185; A.D. acknowledges partial financial support by the Istituto Nazionale di Fisica Nucleare (INFN) through the Iniziativa Specifica RM21 for foreign guests; and by the MICINN through the research project FPA2006-05423 and through the INFN-MICINN-08 Bilateral Agreement (Italy-Spain) "Flavour as a window for new physics"; D.M. acknowledges partial financial support by Ministry of University and of Scientific Research of Italy, through the 2007-08 COFIN program. A.D. and J.L.-P. acknowledge also financial support from the Comunidad Autónoma de Madrid through the project P-ESP-00346. Eventually, A.D., J.L.-P. and D.M. acknowledge the financial support of the European Community under the European Commission Framework Programme 7 Design Study: EUROnu, Project Number 212372; and under the Framework Programme 6 BENE-CARE networking activity MRTN-CT-2004-506395. The EC is not liable for any use that may be made of the information contained herein.

A.D. and J.L.-P. thank the Physics Department of the Università di Roma "La Sapienza", where this work has been completed.

References

- [1] B. T. Cleveland *et al.*, *Astrophys. J.* **496** (1998) 505.
- [2] J. N. Abdurashitov *et al.* [SAGE Collaboration], *Phys. Rev. C* **60** (1999) 055801 [arXiv:astro-ph/9907113].

- [3] W. Hampel *et al.* [GALLEX Collaboration], Phys. Lett. B **447** (1999) 127.
- [4] S. Fukuda *et al.* [Super-Kamiokande Collaboration], Phys. Rev. Lett. **86** (2001) 5651 [arXiv:hep-ex/0103032].
- [5] J. P. Cravens *et al.* [Super-Kamiokande Collaboration], Phys. Rev. D **78** (2008) 032002 [arXiv:0803.4312 [hep-ex]].
- [6] Q. R. Ahmad *et al.* [SNO Collaboration], Phys. Rev. Lett. **87** (2001) 071301 [arXiv:nucl-ex/0106015].
- [7] S. N. Ahmed *et al.* [SNO Collaboration], Phys. Rev. Lett. **92** (2004) 181301 [arXiv:nucl-ex/0309004].
- [8] B. Aharmim *et al.* [SNO Collaboration], Phys. Rev. Lett. **101** (2008) 111301 [arXiv:0806.0989 [nucl-ex]].
- [9] Y. Fukuda *et al.* [Super-Kamiokande Collaboration], Phys. Rev. Lett. **81** (1998) 1562 [arXiv:hep-ex/9807003].
- [10] M. Ambrosio *et al.* [MACRO Collaboration], Phys. Lett. B **517** (2001) 59 [arXiv:hep-ex/0106049].
- [11] M. Apollonio *et al.* [CHOOZ Collaboration], Phys. Lett. B **466** (1999) 415 [arXiv:hep-ex/9907037].
- [12] M. Apollonio *et al.* [CHOOZ Collaboration], Eur. Phys. J. C **27** (2003) 331 [arXiv:hep-ex/0301017].
- [13] F. Boehm *et al.*, Phys. Rev. D **64** (2001) 112001 [arXiv:hep-ex/0107009].
- [14] K. Eguchi *et al.* [KamLAND Collaboration], Phys. Rev. Lett. **90** (2003) 021802 [arXiv:hep-ex/0212021].
- [15] M. H. Ahn *et al.* [K2K Collaboration], Phys. Rev. Lett. **90** (2003) 041801 [arXiv:hep-ex/0212007].
- [16] E. Aliu *et al.* [K2K Collaboration], Phys. Rev. Lett. **94** (2005) 081802 [arXiv:hep-ex/0411038].
- [17] D. G. Michael *et al.* [MINOS Collaboration], Phys. Rev. Lett. **97** (2006) 191801 [arXiv:hep-ex/0607088].
- [18] P. Adamson *et al.* [MINOS Collaboration], Phys. Rev. Lett. **101** (2008) 131802 [arXiv:0806.2237 [hep-ex]].
- [19] C. Amsler *et al.* [Particle Data Group], Phys. Lett. B **667** (2008) 1.
- [20] B. Pontecorvo, Sov. Phys. JETP **6** (1957) 429 [Zh. Eksp. Teor. Fiz. **33** (1957) 549].
- [21] Z. Maki, M. Nakagawa and S. Sakata, Prog. Theor. Phys. **28** (1962) 870.
- [22] B. Pontecorvo, Sov. Phys. JETP **26** (1968) 984 [Zh. Eksp. Teor. Fiz. **53** (1967) 1717].

- [23] V. N. Gribov and B. Pontecorvo, Phys. Lett. B **28** (1969) 493.
- [24] T. Schwetz, M. Tortola and J. W. F. Valle, New J. Phys. **10** (2008) 113011 [arXiv:0808.2016 [hep-ph]].
- [25] G. L. Fogli, E. Lisi, A. Marrone, A. Palazzo and A. M. Rotunno, arXiv:0809.2936 [hep-ph].
- [26] G. L. Fogli, E. Lisi, A. Marrone, A. Palazzo and A. M. Rotunno, Phys. Rev. Lett. **101** (2008) 141801 [arXiv:0806.2649 [hep-ph]].
- [27] H. L. Ge, C. Giunti and Q. Y. Liu, arXiv:0810.5443 [hep-ph].
- [28] M. C. Gonzalez-Garcia and M. Maltoni, arXiv:0704.1800 [hep-ph].
- [29] Y. Itow *et al.* [The T2K Collaboration], arXiv:hep-ex/0106019.
- [30] D. S. Ayres *et al.* [NOvA Collaboration], arXiv:hep-ex/0503053.
- [31] M. Ishitsuka, T. Kajita, H. Minakata and H. Nunokawa, Phys. Rev. D **72** (2005) 033003 [arXiv:hep-ph/0504026].
- [32] K. Hagiwara, N. Okamura and K. i. Senda, Phys. Lett. B **637** (2006) 266 [Erratum-ibid. B **641** (2006) 486] [arXiv:hep-ph/0504061].
- [33] M. V. Diwan *et al.*, Phys. Rev. D **68** (2003) 012002 [arXiv:hep-ph/0303081].
- [34] S. Geer, Phys. Rev. D **57** (1998) 6989 [Erratum-ibid. D **59** (1999) 039903] [arXiv:hep-ph/9712290].
- [35] P. Zucchelli, Phys. Lett. B **532** (2002) 166.
- [36] Belle experiment, <http://belle.kek.jp/>.
- [37] Babar experiment, <http://www-public.slac.stanford.edu/babar/>.
- [38] Y. Grossman, Phys. Lett. B **359** (1995) 141 [arXiv:hep-ph/9507344].
- [39] M. M. Guzzo, A. Masiero and S. T. Petcov, Phys. Lett. B **260** (1991) 154.
- [40] E. Roulet, Phys. Rev. D **44** (1991) 935.
- [41] S. Antusch, C. Biggio, E. Fernandez-Martinez, M. B. Gavela and J. Lopez-Pavon, JHEP **0610** (2006) 084 [arXiv:hep-ph/0607020].
- [42] A. Abada, C. Biggio, F. Bonnet, M. B. Gavela and T. Hambye, JHEP **0712** (2007) 061 [arXiv:0707.4058 [hep-ph]].
- [43] The ISS Physics Working Group, arXiv:0710.4947 [hep-ph].
- [44] T. Ota and J. Sato, Phys. Lett. B **545**, 367 (2002) [arXiv:hep-ph/0202145].
- [45] E. Fernandez-Martinez, M. B. Gavela, J. Lopez-Pavon and O. Yasuda, Phys. Lett. B **649** (2007) 427 [arXiv:hep-ph/0703098];

- [46] G. Altarelli and D. Meloni, Nucl. Phys. B **809** (2009) 158 [arXiv:0809.1041 [hep-ph]].
- [47] C. Athanassopoulos *et al.* [LSND Collaboration], Phys. Rev. Lett. **77**, 3082 (1996) [arXiv:nucl-ex/9605003].
- [48] C. Athanassopoulos *et al.* [LSND Collaboration], Phys. Rev. Lett. **81** (1998) 1774 [arXiv:nucl-ex/9709006].
- [49] A. Aguilar *et al.* [LSND Collaboration], Phys. Rev. D **64** (2001) 112007 [arXiv:hep-ex/0104049].
- [50] LEP Collaborations (ALEPH, DELPHI, OPAL, L3) *et al.*, Phys. Rept. **427** (2006) 257 [arXiv:hep-ex/0509008].
- [51] A. A. Aguilar-Arevalo *et al.* [The MiniBooNE Collaboration], Phys. Rev. Lett. **98** (2007) 231801 [arXiv:0704.1500 [hep-ex]].
- [52] M. Sorel, J. M. Conrad and M. Shaevitz, Phys. Rev. D **70** (2004) 073004 [arXiv:hep-ph/0305255].
- [53] M. Maltoni and T. Schwetz, arXiv:0705.0107 [hep-ph], to appear in PRD.
- [54] V. Barger, D. Marfatia and K. Whisnant, Phys. Rev. D **73**, 013005 (2006) [arXiv:hep-ph/0509163].
- [55] S. Palomares-Ruiz, S. Pascoli and T. Schwetz, JHEP **0509** (2005) 048 [arXiv:hep-ph/0505216].
- [56] A. de Gouvea and Y. Grossman, Phys. Rev. D **74**, 093008 (2006) [arXiv:hep-ph/0602237].
- [57] T. Schwetz, JHEP **0802**, 011 (2008) [arXiv:0710.2985 [hep-ph]].
- [58] A. E. Nelson and J. Walsh, Phys. Rev. D **77**, 033001 (2008) [arXiv:0711.1363 [hep-ph]].
- [59] A. Donini, M. Maltoni, D. Meloni, P. Migliozzi and F. Terranova, JHEP **0712** (2007) 013 [arXiv:0704.0388 [hep-ph]].
- [60] CNGS experiment, <http://proj-cngs.web.cern.ch/proj-cngs/>.
- [61] K. Kimura, A. Takamura and H. Yokomakura, Phys. Lett. B **537**, 86 (2002) [arXiv:hep-ph/0203099].
- [62] K. Kimura, A. Takamura and H. Yokomakura, Phys. Rev. D **66**, 073005 (2002) [arXiv:hep-ph/0205295].
- [63] A. Donini and D. Meloni, Eur. Phys. J. C **22** (2001) 179 [arXiv:hep-ph/0105089].
- [64] A. Donini, M. Lusignoli and D. Meloni, Nucl. Phys. B **624** (2002) 405 [arXiv:hep-ph/0107231].
- [65] T. Abe *et al.* [ISS Detector Working Group], arXiv:0712.4129 [physics.ins-det].

- [66] A. Cervera, A. Donini, M. B. Gavela, J. J. Gomez Cadenas, P. Hernandez, O. Mena and S. Rigolin, Nucl. Phys. B **579**, 17 (2000) [Erratum-ibid. B **593**, 731 (2001)] [arXiv:hep-ph/0002108].
- [67] A. Donini, D. Meloni and P. Migliozzi, Nucl. Phys. B **646** (2002) 321 [arXiv:hep-ph/0206034].
- [68] J. Burguet-Castell *et al.*, Nucl. Phys. B **608** (2001) 301 [arXiv:hep-ph/0103258];
- [69] H. Minakata and H. Nunokawa, JHEP **0110** (2001) 001 [arXiv:hep-ph/0108085];
- [70] A. Donini, M. B. Gavela, P. Hernandez and S. Rigolin, Nucl. Phys. B **574** (2000) 23 [arXiv:hep-ph/9909254].
- [71] A. Donini, M. B. Gavela, P. Hernandez and S. Rigolin, Nucl. Instrum. Meth. A **451** (2000) 58 [arXiv:hep-ph/9910516].
- [72] A. Kalliomaki, J. Maalampi and M. Tanimoto, Phys. Lett. B **469** (1999) 179 [arXiv:hep-ph/9909301].
- [73] A. Dighe and S. Ray, Phys. Rev. D **76**, 113001 (2007) [arXiv:0709.0383 [hep-ph]].
- [74] A. Boyarsky, A. Neronov, O. Ruchayskiy and M. Shaposhnikov, Mon. Not. Roy. Astron. Soc. **370** (2006) 213 [arXiv:astro-ph/0512509].
- [75] M. Maltoni, T. Schwetz, M. A. Tortola and J. W. F. Valle, New J. Phys. **6** (2004) 122 [arXiv:hep-ph/0405172].
- [76] N. Okada and O. Yasuda, Int. J. Mod. Phys. A **12** (1997) 3669 [arXiv:hep-ph/9606411].
- [77] S. M. Bilenky, C. Giunti and W. Grimus, Eur. Phys. J. C **1** (1998) 247 [arXiv:hep-ph/9607372].
- [78] F. Dydak *et al.*, Phys. Lett. B **134** (1984) 281.
- [79] Y. Declais *et al.*, Nucl. Phys. B **434** (1995) 503.
- [80] G. Karagiorgi, A. Aguilar-Arevalo, J. M. Conrad, M. H. Shaevitz, K. Whisnant, M. Sorel and V. Barger, Phys. Rev. D **75**, 013011 (2007) [arXiv:hep-ph/0609177].
- [81] S. M. Bilenky, C. Giunti, W. Grimus and T. Schwetz, Astropart. Phys. **11**, 413 (1999) [arXiv:hep-ph/9804421].
- [82] R. Foot and R. R. Volkas, Phys. Rev. D **55**, 5147 (1997) [arXiv:hep-ph/9610229].
- [83] M. Cirelli, G. Marandella, A. Strumia and F. Vissani, Nucl. Phys. B **708**, 215 (2005) [arXiv:hep-ph/0403158].
- [84] A. De Rujula, M. Lusignoli, L. Maiani, S. T. Petcov and R. Petronzio, Nucl. Phys. B **168** (1980) 54.
- [85] A. M. Dziewonski and D.L. Anderson, Phys. Earth Planet. Int. **25** (1981) 297.

- [86] S. K. Agarwalla, S. Choubey and A. Raychaudhuri, Nucl. Phys. B **771** (2007) 1 [arXiv:hep-ph/0610333].
- [87] A. Bueno, M. Campanelli and A. Rubbia, Nucl. Phys. B **589** (2000) 577 [arXiv:hep-ph/0005007].
- [88] M. Campanelli, A. Bueno and A. Rubbia, Nucl. Instrum. Meth. A **451** (2000) 176.
- [89] A. De Rujula, M. B. Gavela and P. Hernandez, Nucl. Phys. B **547** (1999) 21 [arXiv:hep-ph/9811390].
- [90] A. Broncano and O. Mena, Eur. Phys. J. C **29** (2003) 197 [arXiv:hep-ph/0203052].
- [91] B. Autin, A. Blondel and J. R. Ellis, “Prospective study of muon storage rings at CERN,”
- [92] P. Gruber *et al.*, “The study of a European Neutrino Factory complex.”
- [93] D. Finley and N. Holtkamp, Nucl. Instrum. Meth. A **472**, 388 (2000).
- [94] S. Ozaki *et al.*, BNL-52623, “Feasibility study 2 of a muon based neutrino source.”
- [95] M. M. Alsharoa *et al.* [Muon Collider/Neutrino Factory Collaboration], Phys. Rev. ST Accel. Beams **6**, 081001 (2003) [arXiv:hep-ex/0207031].
- [96] M. S. Zisman, Nucl. Instrum. Meth. A **503**, 384 (2003).
- [97] Y. Kuno, Y. Mori, S. Machida, T. Yokoi, Y. Iwashita, J. Sato and O. Yasuda, “A feasibility study of a neutrino factory in Japan,” <http://www.slac.stanford.edu/spires/find/hep/www?irn=4623622>.
- [98] M. S. Zisman, J. Phys. Conf. Ser. **110** (2008) 112006.
- [99] P. Huber and W. Winter, Phys. Rev. D **68** (2003) 037301 [arXiv:hep-ph/0301257].
- [100] J. Kopp, T. Ota and W. Winter, Phys. Rev. D **78** (2008) 053007 [arXiv:0804.2261 [hep-ph]].
- [101] P. Lipari, private communication.
- [102] P. Lipari, M. Lusignoli and F. Sartogo, Phys. Rev. Lett. **74** (1995) 4384 [arXiv:hep-ph/9411341].
- [103] A. Cervera-Villanueva, AIP Conf. Proc. **981** (2008) 178.
- [104] A. Cervera, F. Dydak and J. Gomez Cadenas, Nucl. Instrum. Meth. A **451**, 123 (2000).
- [105] D. Autiero *et al.*, Eur. Phys. J. C **33** (2004) 243 [arXiv:hep-ph/0305185].
- [106] G. L. Fogli and E. Lisi, Phys. Rev. D **54** (1996) 3667 [arXiv:hep-ph/9604415];
- [107] V. Barger, D. Marfatia and K. Whisnant, Phys. Rev. D **65** (2002) 073023 [arXiv:hep-ph/0112119].
- [108] A. Donini, E. Fernandez-Martinez, D. Meloni and S. Rigolin, Nucl. Phys. B **743** (2006) 41 [arXiv:hep-ph/0512038].

- [109] P. Huber and T. Schwetz, Phys. Lett. B **669** (2008) 294 [arXiv:0805.2019 [hep-ph]].
- [110] E. Ables *et al.* [MINOS Collaboration],
- [111] P. Huber, M. Lindner, M. Rolinec and W. Winter, Phys. Rev. D **74** (2006) 073003 [arXiv:hep-ph/0606119].
- [112] D. Indumathi [INO Collaboration], Pramana **63**, 1283 (2004).
- [113] C. Fukushima *et al.*, Nucl. Instrum. Meth. A **592** (2008) 56.
- [114] D. Meloni, Phys. Lett. B **664** (2008) 279 [arXiv:0802.0086 [hep-ph]].
- [115] P. Migliozzi, private communication.
- [116] L. Scotto Lavina, talk at the NuFact'08 Workshop, Valencia,
<http://indico.ific.uv.es/indico/materialDisplay.py?contribId=132&sessionId=23&materialId=slides&confId=71>.
- [117] K. Fuki, poster at the NuFact'08 Workshop, Valencia,
<http://indico.ific.uv.es/indico/materialDisplay.py?contribId=166&sessionId=38&materialId=poster&confId=71>.
- [118] D. Meloni, arXiv:0812.3555v1 [hep-ph].
D. Meloni, talk at the NOW'08 Workshop, Otranto,
- [119] A. Donini, D. Meloni and S. Rigolin, JHEP **0406** (2004) 011 [arXiv:hep-ph/0312072].
- [120] A. Laing and F. J. P. Soler, AIP Conf. Proc. **981** (2008) 166.
- [121] Z. z. Xing and H. Zhang, Phys. Lett. B **618** (2005) 131 [arXiv:hep-ph/0503118].
- [122] O. Yasuda, arXiv:0704.1531 [hep-ph].
- [123] H. Zhang, Mod. Phys. Lett. A **22**, 1341 (2007) [arXiv:hep-ph/0606040].